Desalination 551 (2023) 116386

Contents lists available at ScienceDirect

Desalination

journal homepage: www.elsevier.com/locate/desal

Investigation of pulsed electric field operation as a chemical-free anti-scaling approach for electrodialysis desalination of brackish water

Soraya Honarparvar [a,*,1], Rashed Al-Rashed [a,b,*,1], Amos G. Winter V. [a]

[a] Department of Mechanical Engineering, Massachusetts Institute of Technology, Cambridge, MA 02139, USA
[b] Department of Mechanical Engineering, College of Petroleum and Engineering, Kuwait University, Kuwait

HIGHLIGHTS

- Pulsed electric field (PEF) can improve scale mitigation in electrodialysis (ED).
- The transport rates of scale-forming ions change when using pulsed operation.
- PEF alters the quantity and morphology of formed crystals.
- PEF parameters need to be adjusted according to water composition.
- Combining pulsed and conventional operation leads to an improved desalination rate.

ARTICLE INFO

Keywords:
Electrodialysis
Scale mitigation
Concentration polarization
Pulsed electric field
Pulsed electrodialysis
Specific energy consumption
Hybrid pulsed-conventional operation

ABSTRACT

Pulsing the electric field is a strategy to mitigate concentration polarization in electrodialysis (ED). To evaluate the effects of the pulsed operation on the extent and kinetics of salt formation, a series of nine-day batch experiments were performed for pulsed and conventional ED (PED and CED, respectively). The pulsing duty cycle was set to 50 % and frequencies of 0.5 and 5 Hz were selected according to the divalent to monovalent ion fluxes calculated using the developed model. The results indicated that membrane scaling decreased in PED, with minimal scaling detected under 0.5 Hz. Concentration polarization moderation and lower supersaturation of the scale-forming ions in boundary layers as well as the removal of formed crystals from the stack during the pausing periods contributed to the reduction in scale formation. Considering that the scale-forming ions were transported to the concentrate channel within the first 50 % of the batch time, a novel hybrid pulsed-conventional operation was theorized that leveraged pulsing early in the batch and switched to constant voltage later to expedite the desalination process. Hybrid operation improved the desalination rate compared to a pure PED system and could potentially reduce membrane scaling by decreasing the recirculation period of the concentrate stream.

1. Introduction

Growing water demands necessitate the development of efficient desalination technologies to facilitate the utilization of saline water resources for accommodating water needs. Low-salinity brackish water is abundant in many water-scarce areas in the US, making it an attractive water resource in these regions. However, the majority of brackish groundwaters, despite sustaining medium to low salinities (total dissolved solid (TDS) < 3000 mg/L) [1], are dominated by scale-forming compounds, e.g., Ba^{2+}, Ca^{2+}, Sr^{2+}, CO_3^{2-}, and SO_4^{2-}, which can precipitate even at low concentrations [2–4]. These inorganic constituents of brackish water should be completely/partially removed through desalination to improve water quality for potable and non-potable applications. The main considerations in selecting the optimum desalination technology for brackish water treatment among existing membrane processes [5] are the energy efficiency of the process for desalination of medium-salinity feedwater as well as its resilience toward membrane scaling.

Electrodialysis (ED) is an electro-membrane desalination technique with lower energy requirements for the treatment of medium-salinity feedwater (TDS < 3000 mg/L) compared to competitive technologies, e.g., reverse osmosis and membrane capacitive deionization [6–8]. ED utilizes an electric field to drive ions through cation and anion exchange

* Corresponding authors.
E-mail addresses: shonar@mit.edu (S. Honarparvar), alrashed@mit.edu (R. Al-Rashed).
[1] Co-first-authors – authors with the same contributions

https://doi.org/10.1016/j.desal.2023.116386
Received 13 August 2022; Received in revised form 23 December 2022; Accepted 8 January 2023
Available online 27 January 2023

Nomenclature

AEM	anion exchange membrane
BL	boundary layer
CBL	concentrate boundary layer
CED	conventional electrodialysis
CEM	cation exchange membrane
CP	concentration polarization
DBL	diluate boundary layer
DR	desalination rate
ED	electrodialysis
IEMs	ion exchange membranes
PED	pulsed electrodialysis
SEC	specific energy consumption

membranes (CEMs and AEMs, respectively), alternately placed between two electrodes (Fig. 1a). An ED cell is the repeating unit of the stack, containing an AEM, a CEM, and two adjacent channels. As feedwater flows in channels between membranes, ions move toward the oppositely-charged electrode. The semi-permeability of ion exchange membranes (IEMs) leads to the net transport of ions from one channel to the adjacent compartments, forming diluate and concentrate streams at the outlet. The higher ionic content of the concentrate channel raises the potential for salt formation and membrane clogging in this compartment. Polarity reversal is the industry-standard operational approach to improving the scaling resistance of ED [9]. In ED reversal (EDR), the polarity of the electric field is periodically switched to allow for alternation of the diluate and concentrate channels in the stack and prevent salt build-up on one side. The low energy consumption and the anti-scaling properties of reversal operation make EDR an attractive technology for brackish water treatment.

The high transport number of counterions through IEMs relative to the bulk solution results in the formation of concentration gradients in the vicinity of the membranes (Fig. 1b). This phenomenon is known as concentration polarization (CP) and leads to high ionic concentrations at the membrane-solution interface in the concentrate channel, raising the potential for surpassing the solubility limits and thus, salt formation on the surface of membranes. The supersaturation ratio is defined as the ions concentrations product over their solubility product and is used to determine the scaling propensity of the solution. A supersaturation ratio greater than unity indicates an unstable solution with the potential for salt precipitation. The salt formation kinetics involves two main steps, nucleation and crystal growth, the rate of each depends on several parameters including the supersaturation ratio of the solution, ionic composition, temperature, surface energy of the membranes, and the duration of the induction time (the period between the onset of supersaturation to salt nuclei formation) [10]. A high supersaturation increases the nucleation rates while low supersaturation results in larger formed crystals [11]. Salt crystals can either directly form on membrane surfaces (heterogeneous crystallization) or in the bulk solution (homogeneous crystallization). The formed crystal in the bulk can deposit on the membrane surfaces, creating a loosely attached cake layer. Scaling on the membranes increases their resistance and reduces the available area for ion transport. Even with polarity reversal, membrane scaling still occurs in EDR and decreases the desalination efficiency of the process [12]. The development of cost-effective and efficient approaches for scale mitigation is the key to further improving the viability of brackish water desalination with ED.

Common strategies to reduce scaling and fouling include membrane surface modification [13], pretreatment of the feed water [14,15], and acid and antiscalant dosing [2]. Laboratory studies indicate that the modification of membrane physical and chemical properties could improve their antifouling/scaling properties [16–18]; however, the large-scale fabrication of such membranes may become costly and cumbersome. The use of pretreatment processes, such as a pellet reactor or filtration techniques, increases the capital cost as well as the energy consumption of desalination. While periodic chemical rinsing of the membranes can be effective in minimizing scaling [2], the use of strong acids can degrade the ion-exchange groups and the polymeric matrix of

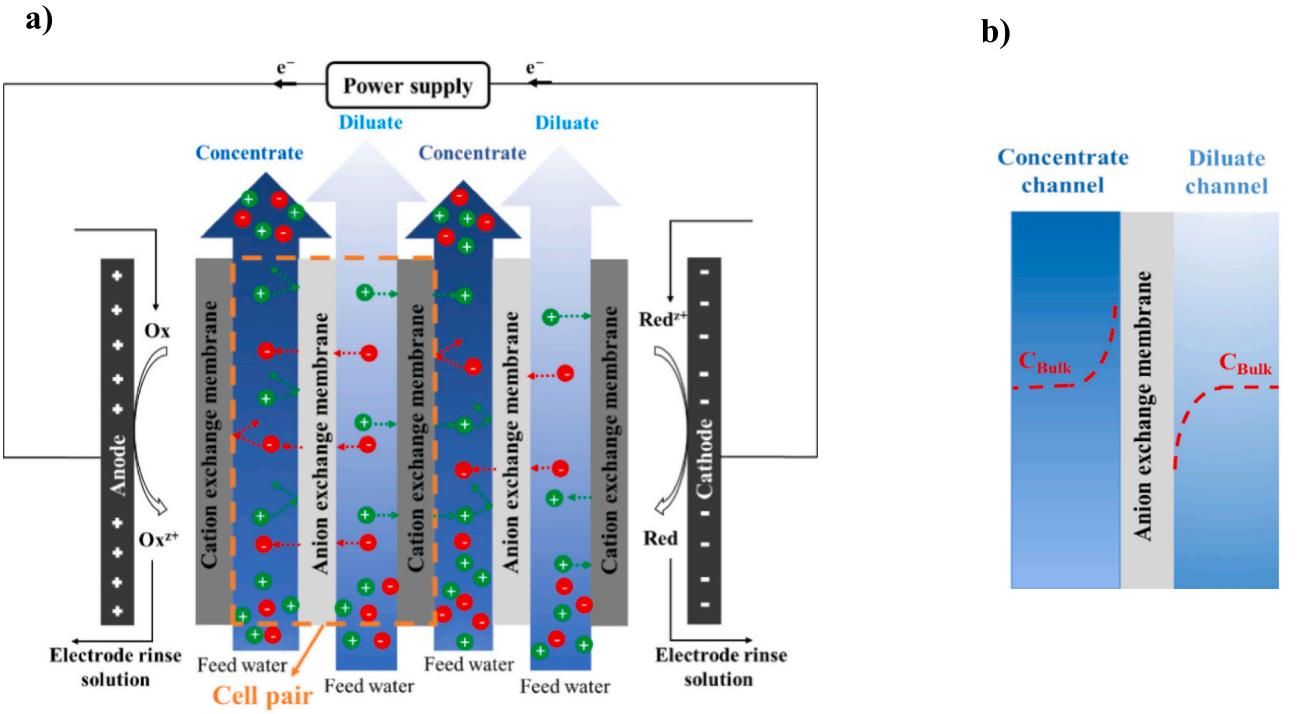

Fig. 1. a) A schematic diagram of the electrodialysis stack. An electrodialysis cell contains an anion exchange membrane, a cation exchange membrane, a concentrate, and a diluate channel. **b)** The formation of concentration gradients in the vicinity of the membranes is known as concentration polarization.

the membrane, reducing membrane lifetime [19,20]. The costs associated with the chemicals, pump, and management of the effluent waste stream are among the many other disadvantages of chemical dosing for fouling/scaling reduction. Hence, the development of low-cost, chemical-free anti-scaling approaches can significantly reduce the operational cost, energy consumption, and complexity of ED for the desalination of brackish water.

Pulsing the electric field is a chemical-free operational strategy to suppress CP and decrease membrane scaling. In pulsed ED (PED), the pulsing period (t_{on}) with an imposed voltage is followed by a pausing period (t_{off}) with zero current density, during which the concentration profiles in the boundary layers (BLs) return back to their bulk value. Due to the dynamic nature of CP, the effectiveness of pulsing for scale mitigation relies on the choice of pulsing temporal parameters including duty cycle ($\alpha = \frac{t_{on}}{t_{on}+t_{off}}$) and frequency ($f = \frac{1}{t_{on}+t_{off}}$).

In prior studies [6,21–39], the use of pulsed operation for scaling/fouling mitigation in ED has been investigated for a diverse range of solution compositions at various pulsing conditions, as summarized in Table A1. While these studies indicated that pulsing under certain conditions reduced membrane fouling/scaling [6,21–33,39] and improved the desalination rate (DR) [21–25,28,31–34,39], they did not provide any guidelines for tuning pulsing parameters for various water chemistries. In these studies, the t_{on}/t_{off} ratios were selected randomly, requiring time-consuming trial-and-error approaches to identify the effective conditions. Furthermore, limited information has been reported on the effects of these parameters on desalination performance and salt formation kinetics. Hence, there is a lack of certainty that pulsing parameters selected for a specific solution composition are effective for other water chemistries.

The lack of generalizable insights on the effects of pulsing parameters becomes a significant limitation when using PED for the desalination of brackish water with regional diversities in salinity and composition [1]. In addition, several prior studies investigated scale mitigation in PED with pH-controlled or non-scale-forming concentrate solutions [21–29,31,33,35–38]. The optimum parameters identified under such conditions do not apply to real desalination units for brackish water treatment which operate with the same feedwater for both the diluate and concentrate streams. To assess the viability of the pulsed operation as a scale mitigation approach for brackish water treatment, the effects of pulsing parameters on specific energy consumption (SEC), DR, and the rates of various steps of salt formation kinetics (nucleation and growth) should be determined. The development of a simple yet generalizable approach for adjusting the temporal parameters of pulsing is necessary to effectively use the process for diverse ranges of water compositions and system sizes.

To address the existing knowledge gap, we developed a theoretical model and built an experimental setup to evaluate the desalination performance and salt formation in PED and conventional ED (CED). The impacts of pulsing on SEC, DR, pH changes of ED in the absence of scale-forming ions were extensively investigated in our previous study using NaCl solution as the feedwater [40]. The insights achieved from our prior work helped narrow down the range of pulsing parameters for scale mitigation experiments. Here, we aimed to elucidate the effects of the pulsed operation on salt formation in ED. Synthesized brackish water with a high scaling propensity was used to compare the scale formation in PED and CED. The long-term, intermittent, batch operation was selected to evaluate the effectiveness of pulsing as a chemical-free, scale-mitigation strategy for medium-scale desalination units that are normally operated under such conditions. The results of this work provide the insights that are essential for developing a systematic approach for tuning pulsing parameters according to feedwater chemistry.

2. Modeling framework

Modeling concentration distribution in the BLs and ionic fluxes across the membranes provide the guideline required for selecting effective pulsing parameters for PED. Here, a brief description of the main equations and assumptions of the 1-D transient ion transport model developed in our prior study [40] is provided. Considering that scale formation is dominant on the surface of the CEM [41], the modeling domains (Fig. 2) for this study only include a CEM and a diluate and a concentrate boundary layer (DBL and CBL, respectively). Ionic fluxes inside BLs and CEM are calculated using the Nernst-Planck (NP) equation

$$N_i^j(x,t) = -D_i^j\frac{dc_i^j(x,t)}{dx} - \frac{D_i^j}{RT}Fz_ic_i^j(x,t)\frac{d\varphi^j(x,t)}{dx}\ j: CBl, DBL, and\ CEM \quad (1)$$

Here, N_i^j, D_i^j, c_i^j, are, respectively, flux, diffusion coefficient, and concentrations of species i in compartment j (DBL, CBL, and CEM); F is the Faraday number (C/mol); z_i is the charge number of species i; and φ^j is the potential in compartment j. The diffusion coefficients of ions inside CEM are estimated using the proposed relationship by Mackie and Mears [40,42] which connects the ionic diffusion coefficient in the solution to those in CEM using the water volume fraction of the membrane. The ionic fluxes described in Eq. (1) are used to derive the molar balance equation (Eq. (2)) for all the existing species. The electroneutrality assumption which states that no space charge forms provides the additional equation (Eq. (3)) required for solving the system of equations to calculate the concentration and potential distributions in the system. The electroneutrality assumption is valid for an ED cell operated at sub-limiting conditions [43] which is the industry-standard operational mode of the process. The electroneutrality inside the membrane accounts for the concentration of fixed charges which for the CEM modeled in this study are considered to be univalent negative ions (charge number of −1).

$$\frac{dc_i^j(xt)}{dt} = \nabla.N_i^j(xt)\ j: CBL, DBl\ and\ CEM \quad (2)$$

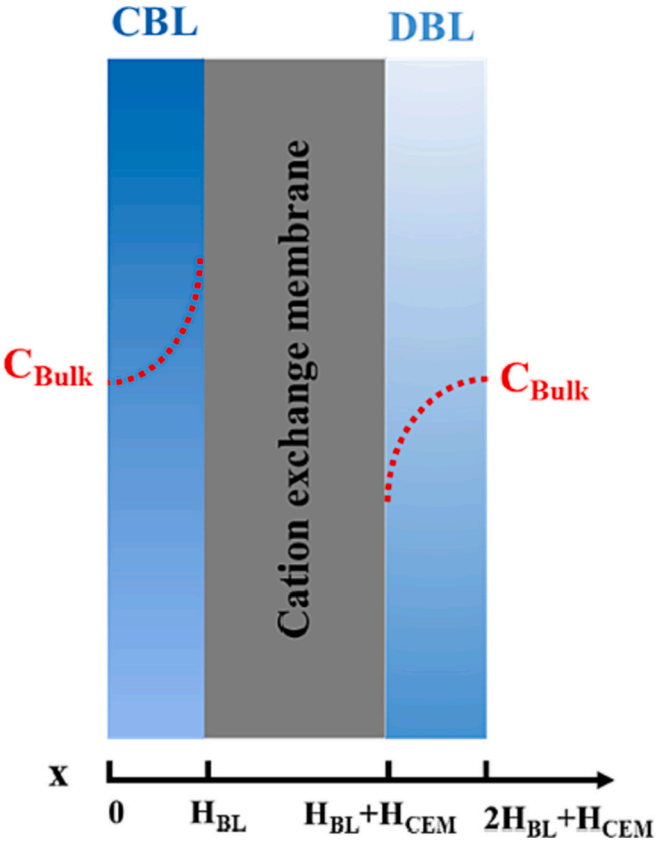

Fig. 2. A schematic diagram of the modeling domains.

$$\sum_i z_i c_i(xt) = 0, in\ CBL\&DBL, i: \text{free ions } in\ CEM, i: \text{free ions and membrane charges} \quad (3)$$

The boundary conditions used to solve the system of equations include continuity of fluxes and current density and Donnan equilibrium (Eq. (4)) at the membrane solution interface.

$$\varphi^{IEM} - \varphi^{channel} = \frac{RT}{Fz_i} ln\left(\frac{c_i^{channel}}{c_i^{IEM}}\right) \quad (4)$$

The system of equations is solved numerically using the finite difference approach with a linear discretization of the domains with a smaller grid size in the BLs. A summary of model input parameters is provided in Table 1.

2.1. The simplified modeled solution chemistry

Ionic compounds in brackish water can be lumped into two main groups, monovalent non-scaling (Na^+, K^+, and Cl^-), and divalent scale-forming (Ca^{2+}, Mg^{2+}, Ba^{2+}, Sr^{2+}, CO_3^{2-}, SO_4^{2-}) ions. The similarities in ionic properties (charge number and diffusion coefficient) in each group is leveraged to simplify the solution chemistry into a ternary system containing Na^+ as the major cation, Mg^{2+} representing all the scale-forming divalent cations, and Cl^- as the major anion. Such simplification was done to reduce the computational time while enabling the investigation of the selective transport of ions across CEM in ED which provides the guideline required for selecting a pulsing frequency for the performed experiments. The concentration ratio of divalent/monovalent ions (cMg^{2+}/cNa^+) in the modeled feedwater was set to 0.4 based on the chemistry of the synthesized brackish water studied here (Table 2). The concentration of Mg^{2+} was selected as the summation of concentrations of Mg^{2+} and Ca^{2+} in the feed water.

The modeled solution chemistry was further simplified to an aqueous binary NaCl solution for the calculation of the boundary resistance. Membrane scaling increases the electrical resistance of an ED cell, leading to a higher SEC of the process. The overall resistance of an ED channel (R_{Ch}) is composed of the resistances of the bulk solution (R_B), boundary layer (R_{BL}), scaling layer (R_S), and membranes (R_M),

$$R_{Ch} = R_B + R_{BL} + R_S + R_M \quad (5)$$

The bulk and boundary resistances of the diluate channel increase throughout the desalination process due to the depletion of ionic concentration. While membrane resistance remains constant throughout a batch since it mainly depends on the concentration of the fixed charges of the membranes. Under an equal diluate concentration, pulsing can affect channel resistance by changing CP and the extent of membrane fouling/scaling. Calculating R_{BL} in the absence of scale-forming ions (using NaCl solution with no divalent ions), helped identify the effects of moderating CP with pulsing on channel resistance and differentiate them from the impacts raised due to the formation of the scaling layer.

Table 1
Model input parameters.

Parameter	Value	Unit
Boundary layers thicknesses, δ	0.045	mm
CEM thickness, H_{CEM}	0.1	mm
Temperature, T	298.15	K
Na^+ diffusion coefficient in water, D_{Na+}	1.33×10^{-9}	m^2/s
Mg^{2+} diffusion coefficient in water, D_{Mg2+}	7.7×10^{-10}	m^2/s
Cl^- diffusion coefficient in water, D_{Cl-}	2.03×10^{-9}	m^2/s
CEM fixed charges concentration, $c_{f,CEM}$	1500	mol/m^3 absorbed H_2O

Table 2
The chemistry of the synthesized brackish water for scale mitigation experiments.

Ion	Mean dissolved solid, mg/L
Na^+	376
Mg^{2+}	60
Ca^{2+}	200
Cl^-	470
HCO_3^-	732
SO_4^{2-}	72

3. Materials, methods, and pulsing parameter selection

3.1. Materials and experimental setup

To investigate the scale mitigation properties of PED, a bench-scale experimental setup (Fig. 3a) with automatic control of system variables was designed and assembled. The system contained two hydraulically isolated diluate and concentrate loops including their feed tanks and the associated sensors as shown in the schematic diagram (Fig. 3b). Since scale formation on the flow spacers increases the pressure drops, a positive displacement peristaltic pump (EW-07522, Cole-Parmer, USA) was used to circulate diluate and concentrate streams through the stack to ensure continued operation at a constant flowrate. A pair of 5 μm filters were installed immediately downstream of the pump to remove larger particles from the solution before entering the ED stack (ED-64002, PCCell, Germany), which contained three cell pairs. Each cell pair included a flow spacer between homogeneous AEM (PC-SA, PCCell, Germany) and CEM (PC-SK, PCCell, Germany) membranes. Pressure accumulators (SFAT-075, SEAFLO, China) were used to avoid pressure fluctuations between the two streams within the ED stack (ED-64002, PCCell, Germany). A diaphragm pump (BYT-7A108, Bayite, China) was used to recirculate a 0.2 mol/L Na_2SO_4 (≥99.0 % purity ACS grade, VWR, USA) solution prepared using distilled water (conductivity ≤5 μS/cm). The pressure (PX-319, Omega, USA), conductivity (CDE-45P, Omega, USA), and pH (PHE-5311, Omega, USA) sensors were installed in the locations shown in Fig. 3b to determine the onset of scale formation as well as evaluating the DR and pH throughout a desalination batch.

Sensor data collection was managed using LABVIEW through data acquisition devices (NI-DAQ 9205, 9208, and 9375, National Instruments, USA) on the controls panel located at the right of Fig. 3a. Within the control panel, a buck converter (DPS5005, Ruideng, China) connected to a 48 V power supply (RSP-750-48, Meanwell, Taiwan) was used to control and measure the voltage relayed to the stack. Frequency control and high-frequency current measurement were performed by a MOSFET (RFP30N06LE, Fairchild Semiconductor, USA) and a current sensor (ACS723, Allegro, USA), placed in series with the ED stack.

3.2. Desalination experiments

Batch desalination experiments were conducted for both PED and CED using synthesized brackish water with chemistry described in Table 2. The scale-forming feedwater was made using $NaHCO_3$ (Macron ≥99.7 % purity ACS grade, Avantor, USA), $CaCl_2$ (≥96.0 % purity ACS grade AMRESCO, Avantor, USA), $CaSO_4$-$2H_2O$ (≥99.0 % purity, Thermo Fisher Scientific, USA), $MgCl_2$-$6H_2O$ (BDH ≥ 99.0 % purity ACS grade, Avantor, USA), and deionized (DI) water. The starting and final salinities of all batches were 2000 and 250 mg/L, respectively. "Each batch desalination experiment was considered complete once the target salinity was reached according to the conductivity sensor located at the diluate stream stack output. The "batch time" (or "desalination time") was calculated as the time elapsed from batch start to batch completion. The experiments were performed with an applied voltage of 4.5 V, a water recovery ratio of 80 %, and a recirculation flowrate of 9 L/h for both the diluate and concentrate streams. Pulsing parameters (duty

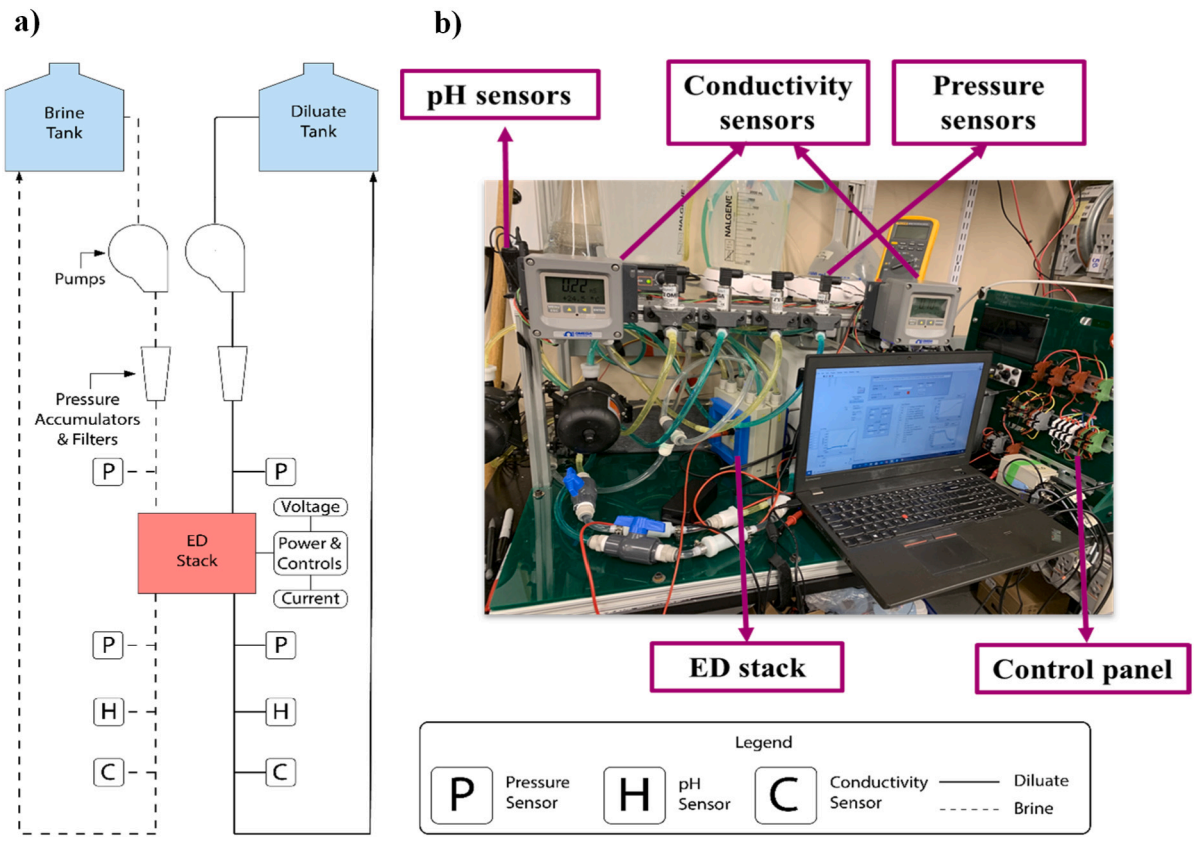

Fig. 3. Constructed experimental setup. **a)** The image of the unit including hydraulic parts, sensors, and electrical panel. **b)** A schematic diagram of the hydraulic components of the experimental setup.

cycle, frequency, and voltage) were selected using a combination of insights gained from studying the desalination performance of PED in the absence of scale-forming ions [40] as well as the modeling results developed for the simplified aqueous ternary solution of Na^{+}-Mg^{2+}-Cl^{-} as described in the subsequent section.

A single desalination experiment with a diluate tank volume of 3 L was performed daily for nine consecutive days to investigate the effects of the long-term, intermittent operation on scale formation. For the last four days of each batch set, water samples were taken from both the diluate and concentrate outlets every 60 min, including the start and end of each batch. The water samples were further analyzed to evaluate the evolution of each species' concentration in channels. The daily cleaning procedure at the end of each batch included flushing the stack with 8 L of distilled water followed by 2 L of 250 mg/L NaCl solution which remained in the stack overnight. Prior to initiating each batch experiment, the stack was flushed with 6 L of synthesized brackish water, followed by 15 min of recirculation of the feed solution through the stack to ensure approximately similar starting conductivities for all nine days.

The SEC of each batch was calculated as $SEC = \frac{\int U(t)I(t)dt}{V_{batch}}$, where V_{batch} describes the volume of the batch. At the end of each nine-day experiment, the middle concentrate channel cell pair (including a CEM, a spacer, and an AEM) was extracted from the stack and dried in atmospheric conditions under the fume hood. The surface of the dried membranes and spacer were further characterized to identify the extent, morphology, and composition of the formed crystals.

3.2.1. Selection of pulsing duty cycle and voltage

In this study, α was set to 50 % to avoid significant decreases in production rate due to pausing periods [40]. In large-scale operations, the longer desalination time increases the required pumping energy, further decreasing the energy efficiency of the process and reducing the viability of pulsing for scale mitigation. Our previous study [40] indicated that a duty cycle of 50 % increased the desalination time by only 60 % while a duty cycle of 20 % resulted in up to a 300 % increase in the desalination time. Hence, the duty cycle of 50 % was selected for the desalination experiments with the synthesized brackish water.

The imposed pulsing voltage for the scale mitigation experiments was set to $0.7U_{lim,\ CED}$ at the target salinity (which was 4.5 V for the conducted experiments in this study). The choice of input voltage was conservative to ensure that water dissociation due to intensified local CP formation as a result of membrane clogging was avoided. Both PED and CED were operated with the same voltage since, as determined in our prior work, increasing the input voltage during the pulsing periods of PED significantly intensified its energy consumption compared to CED and reduced the effectiveness of pulsing for suppressing CP [40].

3.2.2. Selection of pulsing frequency

Pulsing frequency was selected according to the experimental ED stack size and operating flowrate combined with the modeling results of ionic transport fluxes across the CEM (Fig. 4a) calculated for the aqueous ternary solution of Na^{+}-Mg^{2+}-Cl^{-} with divalent/monovalent ions concentration ratio of 0.4 (same as the feed water) at the sub-limiting regime. The concentration of Mg^{2+} was considered to be the summation of existing divalent cations concentrations in the studied feedwater in the experimental section (Table 2). The greater charge number of divalent ions results in their higher transport rates across the membranes compared to monovalent ions. These greater transport rates combined with low mobilities of divalent ions lead to decreases in their concentrations in the DBL where diffusion and electromigration are the main transport mechanisms. Fig. 4b demonstrates that the divalent to monovalent ions concentration ratio at the membrane-solution interface in the diluate channel decreases over time, eventually leading to

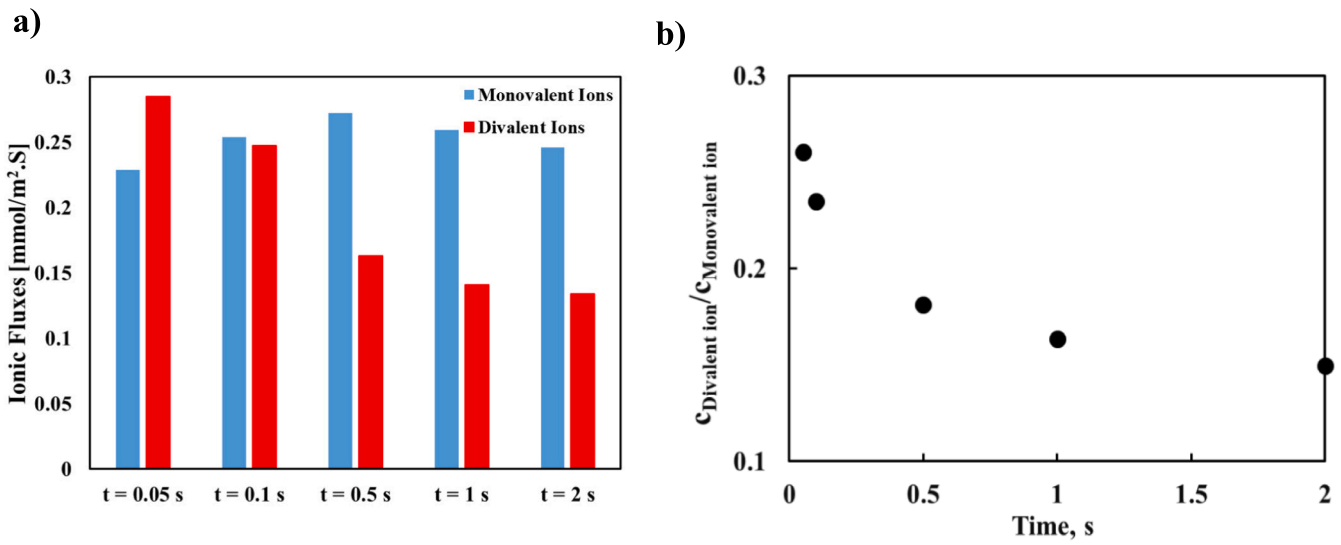

Fig. 4. Selective transport of ions across the membranes in ED. **a)** Comparison of calculated transport fluxes of divalent and monovalent cations fluxes at the CEM-solution interface for the aqueous ternary solution of Na^+-Mg^{2+}-Cl^- with cMg^{2+}/cNa^+ concentration ratio of 0.4 at sub-limiting regime. **b)** Calculated divalent ions to monovalent ions concentration ratios at the membrane-solution interface in the diluate channel. At t = 0, ion concentrations in the boundary layer are assumed to be uniform and equal to the concentrations in the bulk.

reduced transport rates of divalent ions and increased transport rate of monovalent ions across the membrane. Divalent ions (Mg^{2+}) fluxes are greater or equal to that of monovalent ions (Na^+) up to 0.1 s (Fig. 4a). Pulsing with an on-period of 0.1 s (frequency of 5 Hz at the duty cycle of 50 %) results in greater selective transport of divalent ions to the concentrate channel during the on-time, potentially leading to a higher supersaturation and salt nucleation rate in the CBL. However, the removal of formed nuclei from the stack by the longitudinal flow during the off period may still reduce membrane scaling compared to CED.

According to the void channel velocity in the conducted experiments (4.5 cm/s) and the length of the ED stack (8 cm), the residence time of the solution inside the channel is approximately 2 s. Pulsing or pausing periods longer than 2 s may result in scenarios under which the entire residence time of the solution inside the stack is spent either under pulsing or pausing conditions, minimizing the effects of the pulsed operation on modulating CP. The considerations of residence time and the duty cycle of 50 % allow for a maximum on- and off-times of 1 s (0.5 Hz). Pulsing with a frequency of 0.5 Hz may result in lower supersaturation of the CBL with respect to scale-forming ions due to higher monovalent ion transport fluxes for 90 % of the on-time (Fig. 4a). Furthermore, the characteristic time of diffusion (δ^2/D_i) for divalent ions is ~2.6 s. Therefore, a 1 s off-period of 0.5 Hz pulsing provides a better boundary concentration recovery compared to a 0.1 s off-time of 5 Hz, further lowering the concentration of divalent ions in CBL. However, such retrieval in boundary concentrations is accompanied by higher bulk concentrations in the concentrate channel. It is speculated that in PED with the frequency of 0.5 Hz, the relatively long pausing periods during the off-time prevent crystal growth and attachment to the surface of the membranes by retarding the ion transport to the BLs and removing the emerged nuclei from the stack by the longitudinal flow. However, higher recovery of boundary concentration may promote bulk crystallization under 0.5 Hz operation. We selected 0.5 and 5 Hz for desalination experiments in this study to validate these hypotheses and provide a better evaluation of the pulsing effects on various steps of salt formation kinetics.

3.3. Microscopic and spectroscopy analyses

Upon completion of each experiment, the removed AEM, CEM, and spacer were set to dry overnight. Each cell pair component was then inspected and imaged using a microscope (SM-4NTP and HD200VP-UM, Amscope, USA). To remove the loosely adhered particles, the AEM was lightly shaken manually for a minimum of 5 min until no visually significant amount of particles were separated from the membrane any further. Two segments of each membrane in the vicinity of the middle ports, one from the diluate and another from the concentrate side, were extracted and gold-coated for 60 s. Scanning electron microscopy (SEM) was conducted on these samples (Sigma 300 VP, Zeiss, Germany) by applying a 2 kV accelerating voltage at a working distance of 13 mm. The compositions of the formed crystals were identified through conducting energy-dispersive x-ray spectroscopy (EDX) under an accelerating voltage of 20 kV and a working distance of 10 mm (JSM 6010LA, JEOL Ltd., Japan). The composition of the water samples taken during the nine-day experiments was determined through the use of Inductively Coupled Plasma – Optical Emission Spectrometry (ICP-OES). Water samples of diluate and concentrate streams were diluted to 10 and 30 ppm, respectively, using a 3 % HNO_3 solution made with HNO_3 (1 M, Inorganic Ventures, USA) and DI water. The diluted water samples were analyzed using ICP-OES equipment (5800 ICP-OES, Agilent, USA) with the sodium, calcium, magnesium, and sulfur standards (Na/Ca/Mg/S -100PPM-125ML, Inorganic Ventures, USA).

4. Results and discussion

The variation of the operational conditions changes the evolution of ionic concentration distributions in the concentrate channels during a batch, leading to different quantities and morphologies of precipitating crystals. While membrane imaging, as well as pressure drop and SEC measurements, provided an estimation of the quantity and mechanisms of salt formation (homogeneous or heterogeneous), evaluating the concentrate channel ionic compositions (ICP-OES measurements) helped illustrate the potential phenomena that led to the observed variations in the amount and morphology of the precipitating salts. The experimental results described here are used to further assess the viability of the pulsed operation as a chemical-free, scale-mitigation technique.

4.1. Pressure drop during a batch

Attachment of the colloidal particles, e.g., salt crystals, to the spacer

mesh blocks the flow path, increasing the pressure drop in channels. Fig. 5a demonstrates the experimentally measured daily-averaged concentrate channel pressure drop for each desalination batch. The daily-averaged pressures of the concentrate compartment increased throughout the 9 days, indicating that spacer clogging occurred in this channel. The microscopic image of the dried concentrate channel spacer removed from the stack at the end of the nine-day batch experiments under PED with the frequency of 5 Hz indicated that salt particles were attached to the spacer screen, blocking the flow path (Fig. 5b). The concentrate channel spacers used in other operational conditions were partially clogged as well. However, the higher daily-averaged pressure of PED with the frequency of 0.5 Hz indicated greater spacer clogging which could be resulted from potentially higher bulk crystallization in the concentrate channel under this operational condition. The diluate spacers removed from the stack under all operational conditions were clean, consistent with the constant daily averaged pressure drops measured for diluate channels.

4.2. Energy consumption and desalination time

Scaling on the membrane increases its resistance, leading to higher energy consumption in ED. Figs. 6a and b, respectively, present the experimentally measured SECs and batch time of CED and PED with frequencies of 0.5 and 5 Hz. Among all the tested operational conditions, the SEC of PED with the frequency of 0.5 Hz was the lowest for most days of the nine-day experiment. The fluctuations in the measured SEC could be a result of the formation and partial removal of the scaling layers on the surface of the membranes during the desalination or post-cleaning steps at the end of the process. The measured conductivities of the diluate channel at the start of the batch were similar under all operational conditions and the daily deviations were within 1 %, indicating that the variations in SECs of different modes were not due to different quantities of transported ions from diluate to concentrate compartments. The smaller SEC of PED with the frequency of 0.5 Hz even with ~90 % higher desalination time (Fig. 6b) compared to CED demonstrated that the low-frequency pulsing potentially reduced membrane scaling relative to the conventional operation.

The higher measured SEC at the frequency of 5 Hz compared to that of PED with the frequency of 0.5 Hz indicated a larger total cell resistance, which could either be a result of higher membrane scaling or differences in BLs resistances. To elucidate which of these phenomena led to the observed SEC results, the DBL resistance in CED and the cycle-averaged DBL resistance in PED were calculated at target salinity (diluate bulk concentration of 4.3 mol/m^3 NaCl) in the absence of scale-forming components (Fig. 7). As indicated in Fig. 7, pulsed operation results in lower DBL resistance compared to that of CED due to mitigation of CP. Increasing the frequency of pulsing further reduces the DBL resistance due to the shorter on-periods. The calculated DBL resistance suggests that the SEC of PED with a frequency of 5 Hz should be lower than that at 0.5 Hz in the absence of scale precipitating components. These results provide an important benchmark to assess the relative severity of scale formation at different frequencies once scale precipitating components are introduced (as performed experimentally). Considering the lower boundary resistance in PED with a frequency of 5 Hz, the higher SEC under this condition suggests that more membrane scaling occurred compared to that in PED with the frequency of 0.5 Hz.

4.3. Microscopic and spectroscopy results

The morphological and elemental analyses of the crystals formed on the surface of the membranes helped develop a deeper understanding of the mechanisms and the extent of salt formation under various operational conditions. Fig. 8a–i present pictures and SEM images of concentrate sides of CEMs removed from the stack at the end of the nine-day experimental period. A thin, non-homogeneous, sparsely-distributed scaling layer was formed on the surface of membranes, with a higher thickness in the vicinity of the entry and outlet ports (Fig. 8a–c). The thinnest and most scattered scaling layer was observed on the surface of the CEM used in PED with the frequency of 0.5 Hz, while the thickest and densest scaling layer was detected on the surface of the membrane used in CED. The SEM images of membranes (Fig. 8d–i) also verified the formation of denser salt colonies on the surface of the CEM used in CED compared to those of PEDs.

The precipitating salts formed needle-like, floral, and rhombohedral structures. In prior studies [10,44–46], the rhombohedral structure was mainly reported for calcite ($CaCO_3$) [45,47] while the needle-like and floral assemblies were observed for both gypsum ($CaSO_4.2H_2O$) and aragonite (a less thermodynamically stable anhydrous polymorph of $CaCO_3$). The conducted EDX elemental analyses to identify the composition of these floral assemblies demonstrated significant peaks for C, Ca, and O while no major peak was detected for S (Fig. 9), suggesting that these structures were composed of aragonite. The result of EDX analyses was consistent with the calculated saturation index (SI) < 1 for $CaSO_4$ using the ICP-OES data of the ionic compositions of the concentrate stream under all operational conditions, verifying that the bulk solution remained undersaturated with respect to $CaSO_4$ even at the end of the

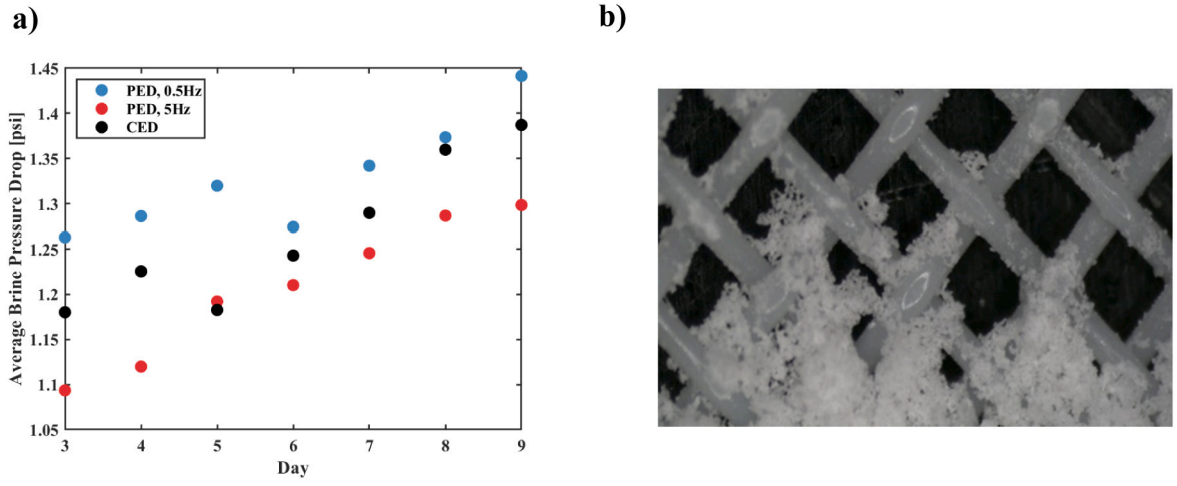

Fig. 5. Evaluation of spacer clogging under various operational conditions. **a)** Experimentally measured daily-averaged pressure drop of the concentrate channels for batches conducted with an imposed voltage of 4.5 V, using synthesized brackish water. PED conditions include frequencies of 0.5 and 5 Hz and the duty cycle of 50 %. **b)** Microscope image (4.5× magnification) of the concentrate channel spacers extracted from the PED system with the frequency of 5 Hz, duty cycle of 50 %, and operating voltage of 4.5 V.

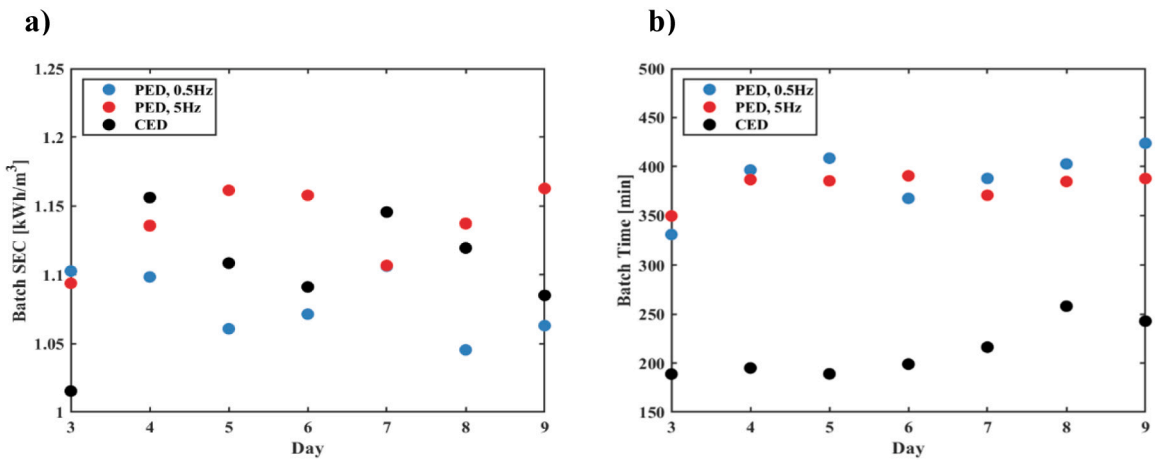

Fig. 6. Comparison of experimentally measured specific energy consumption and batch time of PEDs and CED during day three to day nine of the nine-day experiment with synthesized brackish water, **a)** Specific energy consumption. **b)** Batch time. Input voltage of 4.5 V, pulsing frequencies of 0.5 (●) and 5 Hz (●), and duty cycle of 50 %.

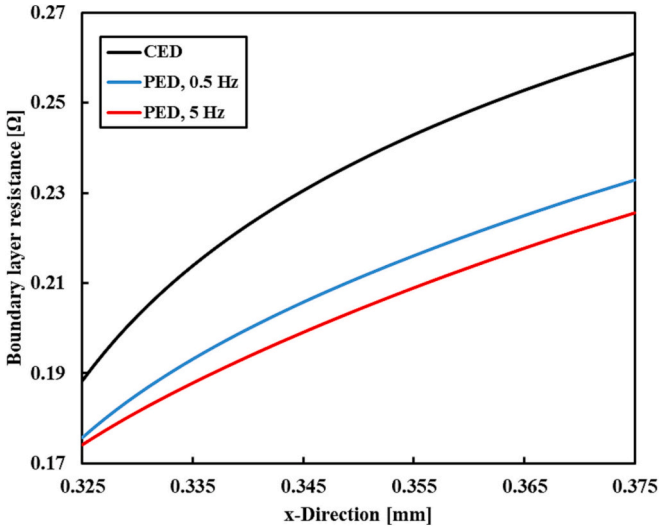

Fig. 7. Calculated modeling results of BL resistance at the end of the batch in CED and cycle-averaged BL resistance in PED with frequencies of 0.5 and 5 Hz and duty cycle of 50 % using NaCl solution as the feedwater.

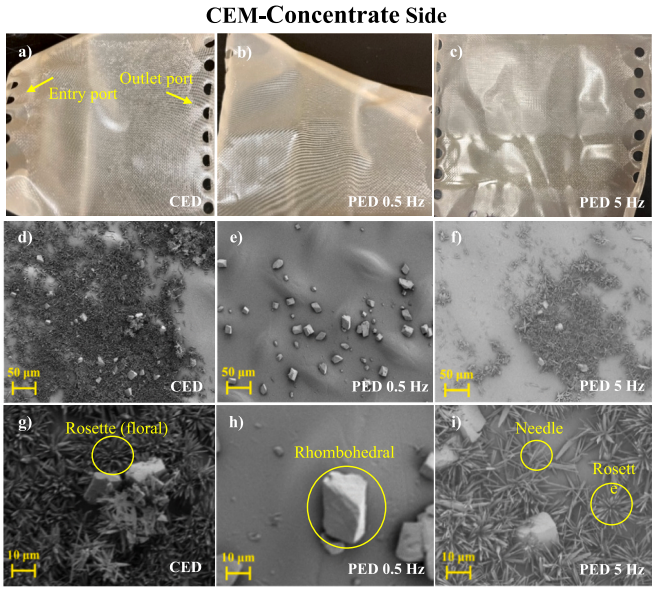

Fig. 8. Photographs **(a–c)** and SEM images **(d–i)** of the concentrate side of the CEM at the end of nine-day experiments with synthesized brackish water. **a, d, g)** CED, **b, e, h)** PED with the 0.5 Hz frequency, and **c, f, i)** PED with the 5 Hz frequency. The duty cycle of PED was set to 50 % and the imposed voltage in all operational modes was 4.5 V.

experiment. The dominance of a specific crystal morphology formed on the surface of the membrane varied depending on operational modes (conventional or pulsed) and pulsing frequency. As indicated in SEM images presented in Fig. 8d–i, the lower quantities of the floral and needle-like structures in pulsed operation elucidated that the aragonite formation was reduced in PED. At the frequency of 0.5 Hz, the precipitating crystal was mainly rhombohedral with a size <20 μm, indicating the formation of thermodynamically-stable calcite crystals.

The pictures (Fig. 10a–c) of the concentrate sides of the dried AEMs showed the formation of a loosely attached, non-homogeneous cake layer under all operational modes, with the maximum thickness of the layer observed for PED with the frequency of 0.5 Hz. Fig. 10d–i present the SEM images of the AEM after removing the loosely adhered salt layers by lightly shaking the membranes. The comparison of the SEM images demonstrated that the salt colonies detected on the surface of the AEM used in CED were larger with needle-like, floral, and rhombohedral crystal assemblies. The EDX spectra (Fig. 11b) of the floral structure indicated major peaks for Ca, C, and O while no significant peak was observed for S, revealing that aragonite was the building component of these crystals. In PED, in addition to the decrease in density of salt colonies, the dominancy of rhombohedral crystals on the surface of the AEM indicated that the formation of thermodynamically stable calcite was prominent, similar to the results observed for the CEM. The significantly lower salt colonies detected in the SEM images of PED with the frequency of 0.5 Hz (Fig. 10e and h) after removing the loosely attached salt layer determined that surface crystallization was minimized under this operational condition.

The SEM images and EDX elemental analyses performed on the removed powder from AEMs used in CED and PED (Fig. 12a–f) with the frequency of 0.5 Hz determined the formation of large rhombohedral polycrystals (up to 100 μm) with rough surfaces combined with smaller needle-like assemblies. The polycrystalline detected in the powder removed from CED was smaller than that of PED. The corresponding EDX elemental maps of both samples, shown in Fig. 12b-c-e-f, revealed that the powder contained high quantities of Ca in the area of bulky polycrystals and a negligible percentage of S which mainly existed in the

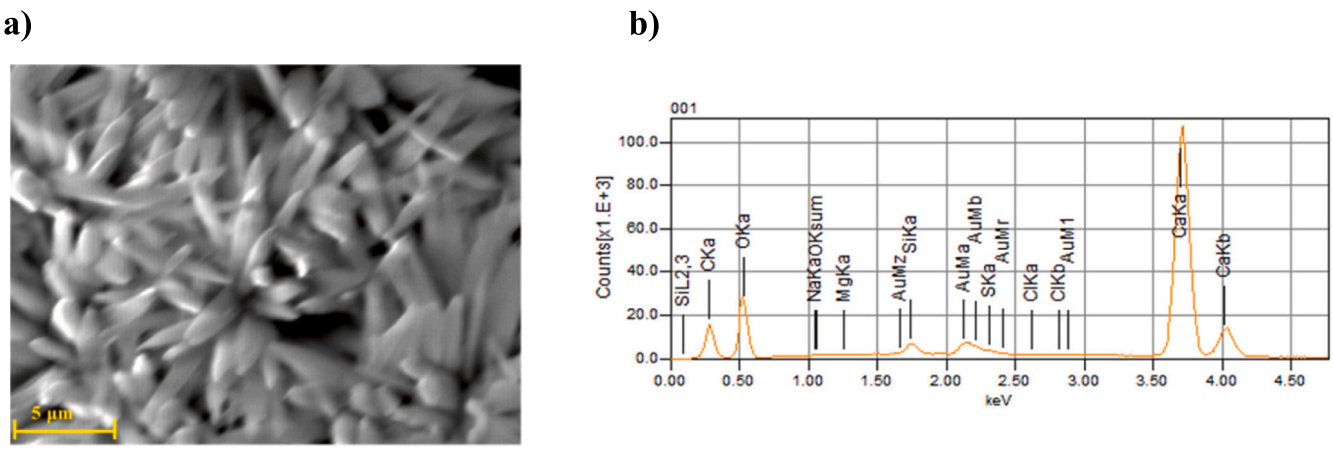

Fig. 9. Characterization of floral crystals formed on the surface of CEM. **a)** SEM image, **b)** EDX spectra of the floral crystals formed on the concentrate side of the CEM used in CED. The EDX spectra identified that these structures contained oxygen, carbon, and calcium which are the producing elements of $CaCO_3$ (aragonite).

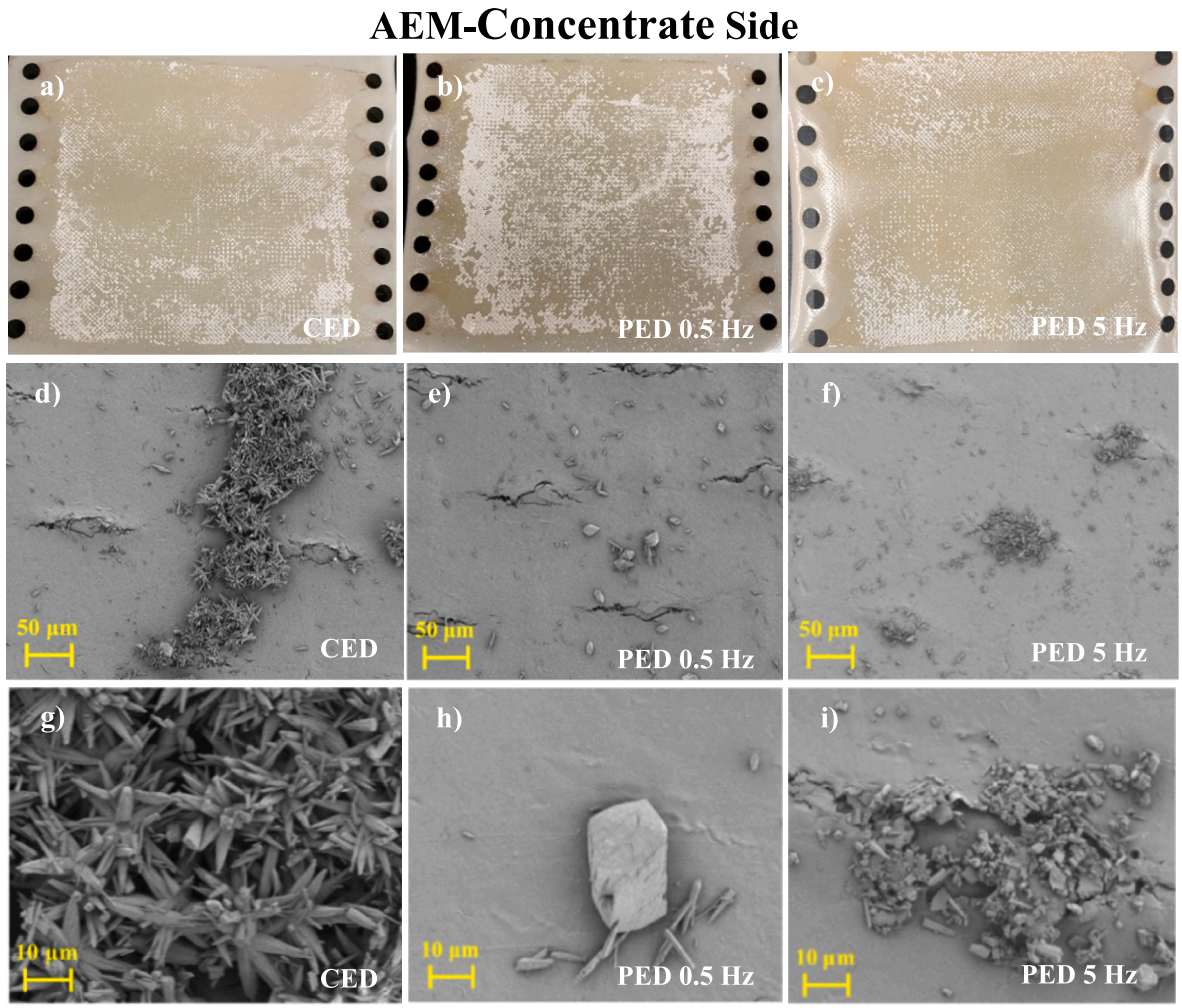

Fig. 10. Photographs **(a–c)** and SEM images **(d–i)** of the concentrate side of the AEM at the end of the nine-day experiments with the synthesized brackish water. **a, d, g)** CED, **b, e, h)** PED 0.5 Hz, and **c, f, i)** PED 5 Hz. The duty cycle of PED was set to 50 % and the imposed voltage in all the operational modes was 4.5 V.

regions with the needle-like smaller crystals. The lack of S in the structure of crystals suggested that the powder mainly contained $CaCO_3$. Hence, the loosely attached salt layer on the surface of the AEM was more likely formed due to the homogeneous bulk crystallization of calcite and its deposition onto the surface of AEM rather than a heterogeneous surface crystallization which appeared to be more dominant for CEM. Such results were consistent with the high supersaturation degree of the synthesized brackish water with respect to $CaCO_3$ which further increased in the concentrate compartment throughout the desalination process, potentially promoting homogenous crystallization and dispersion of formed salt particles. The experimental measurements conducted by Moulin and Roques [48] indicated that $CaCO_3$ crystals

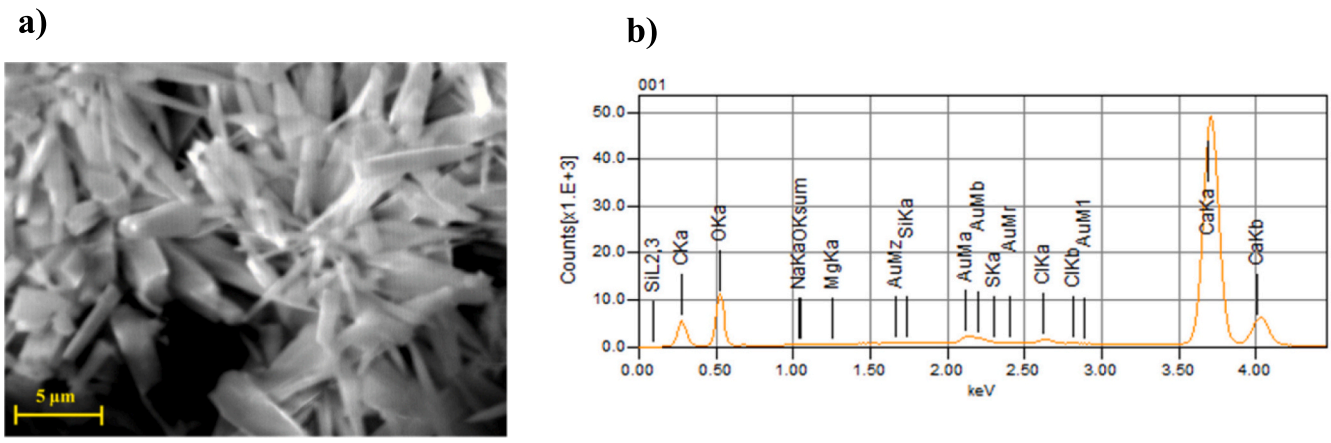

Fig. 11. Elemental analysis of the floral crystals formed on the concentrate side of the AEM used in CED. **a)** SEM image, **b)** EDX spectra. The existing peaks for O, C, and Ca in EDX spectra determined that the floral structures were mainly made of aragonite.

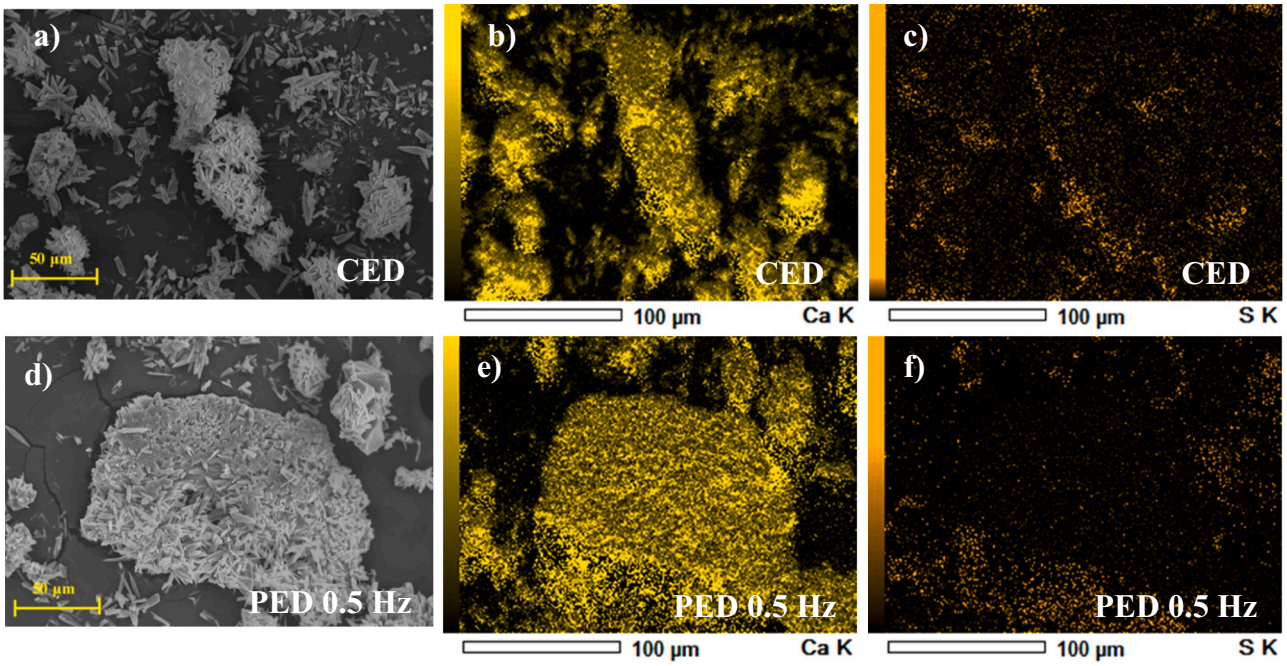

Fig. 12. SEM images and EDX elemental analyses of the powder collected from the surface of the AEM used in CED **(a–c)** and PED **(d–f)** with the frequency of 0.5 Hz.

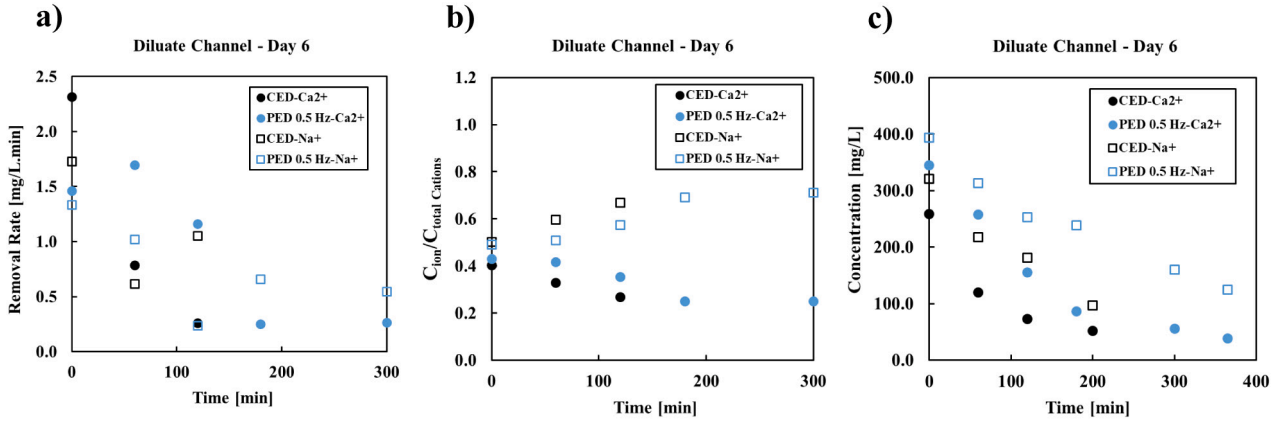

Fig. 13. Evaluation of the effects of 0.5 Hz pulsing on the evolution of solution composition during day six of the nine-day desalination batch experiments. Comparison of (**a**) Ca^{2+} and Na^{+} removal rates, (**b**) Ca^{2+} and Na^{+} concentration ratio relative to existing cations, and (**c**) Ca^{2+} and Na^{+} diluate bulk concentrations.

sustained negative surface charges. Hence, the electrostatic attraction between the negatively charged suspended $CaCO_3$ crystals in the bulk solution and positively charged functional groups of the AEM resulted in their attachment onto the surface of the AEM, forming a cake layer. The higher thickness of the formed cake layer on the surface of the AEM used in PED with the frequency of 0.5 Hz (Fig. 10b) and the larger size of the formed calcite crystals (Fig. 12d) determined that homogeneous nucleation and crystal growth were higher under this operational mode.

4.4. Analyses of the solution composition evolution

ICP-OES measurements of solution composition were employed to calculate transport rates of Na^+ and Ca^{2+} ions from the diluate compartment during a batch. Ion removal rates from the diluate channel are calculated as (where c_i^t and $c_i^{t+\Delta t}$, respectively, represent the concentration of species i at time t and $t+\Delta t$. The comparison of ion removal rates indicates the effects of pulsing with different frequencies on the selective transport of scale-precipitating ions across the membranes. Fig. 13a–c provide, respectively, the removal rate, concentration ratio over existing cations (Na^+, Mg^{2+}, and Ca^{2+}), and concentration in the diluate channel of Ca^{2+} and Na^+, in PED with the frequency of 0.5 Hz compared to those of CED during day six of the desalination experiments. Fig. 14a–c present the comparative results for CED and PED with the frequency of 5 Hz during day seven of the nine-day experiments. Since the initial concentrations of the species in the feedwater can significantly affect their removal rates, the compared days were selected carefully to ensure minimal deviations in the feedwater composition of PED and CED systems. The removal rates of Ca^{2+} in both PED and CED were greater than Na^+ at the start of the batch (Figs. 13–14a), even with the initial concentrations of Ca^{2+} being slightly lower than Na^+ (Figs. 13–14c). Such greater removal rates were due to the higher charge number of divalent ions which resulted in their greater partitioning at the membrane-solution interface (Eq. (4)), increasing the selectivity of ED toward their transport. The greater transport rate of Ca^{2+} led to decreases in its concentration ratio in the diluate channel (Figs. 13–14b), lowering the selectivity of the process toward their transport as the batch progressed. The concentration of Ca^{2+} in the diluate compartment reached its final value approximately within the first 50 % of the batch duration in both conventional and pulsed operations.

The supersaturation degree of the solution affects salt formation kinetics. As indicated in Fig. 13a, pulsing with the frequency of 0.5 Hz reduced the removal rates of both Ca^{2+} and Na^+ ions from the diluate channel during the first 60 min of the batch. The reduction in removal rates of scale-forming Ca^{2+} ions in PED with the frequency of 0.5 Hz could potentially lower supersaturation degrees in the CBL, decreasing the salt nucleation rate. The transport of Ca^{2+} from the CBL to the concentrate bulk solution during the long pausing periods (1 s) could further reduce its concentration in the concentrate boundaries, leading to lower surface crystallization and salt colonies on the membranes (Fig. 8e and h). Note that higher removal rates from diluate channel at any time step were accompanied by greater depletion in ionic concentration ratios in the diluate compartment (Fig. 13b), resulting in decreases in removal rates during the subsequent time step (Fig. 13a).

The concentration of Ca^{2+} in the concentrate channel in PED with the frequency of 0.5 Hz within the second hour of desalination was smaller than that of the CED (Fig. 15a), despite its higher transport rate from the diluate channel. This could be a result of higher bulk crystallization, which occurred in PED with the frequency of 0.5 Hz, lowering the Ca^{2+} concentration in the solution. Transport of Ca^{2+} ions from CBL to the bulk solution during the long pausing period potentially promoted such higher bulk crystallization of calcite. The intensified spacer clogging and pressure drop for PED with the frequency of 0.5 Hz (Fig. 5a), further could verify greater salt formation in the bulk solution.

In PED with the frequency of 5 Hz, the removal rates of Ca^{2+} from the diluate channel were marginally affected while Na^+ were transported with significantly lower rates compared to that of CED (Fig. 14a). Considering that each 60 min time interval in PED (at $\alpha = 50$ %) includes as much active desalination time as 30 min of conventional operation, the equal removal rates of Ca^{2+} in both PED and CED indicated that its transport during the on-periods of pulsing was significantly higher than that of CED. The higher transport rate of scale-forming Ca^{2+} ions to the concentrate compartment increased the supersaturation degree of the CBL during the on-time, potentially resulting in greater salt nucleation rates while lowering the crystal growth rates. However, the removal of the emerged nuclei with the longitudinal flow during the off-times led to reductions in surface crystallization relative to CED (Figs. 8 and 10) even with the higher supersaturation degree of the CBL during the on-periods. The greater salt nucleation rates could decrease the concentration of Ca^{2+} in the concentrate channel due to the separation of ions from the solution. Fig. 15b indicates that Ca^{2+} concentration in the concentrate channel in PED with the frequency of 5 Hz was slightly lower than that of CED. The potentially lower crystal growth rate in PED with the frequency of 5 Hz compared to that of PED with the frequency of 0.5 Hz could be the reason for the generation of smaller crystals in the bulk solution (Fig. 12), leading to decreased spacer clogging and the thickness of the formed cake layer on the surface of the AEM as presented in SEM images (Fig. 10).

The variations in transport rates of ions from diluate to concentrate

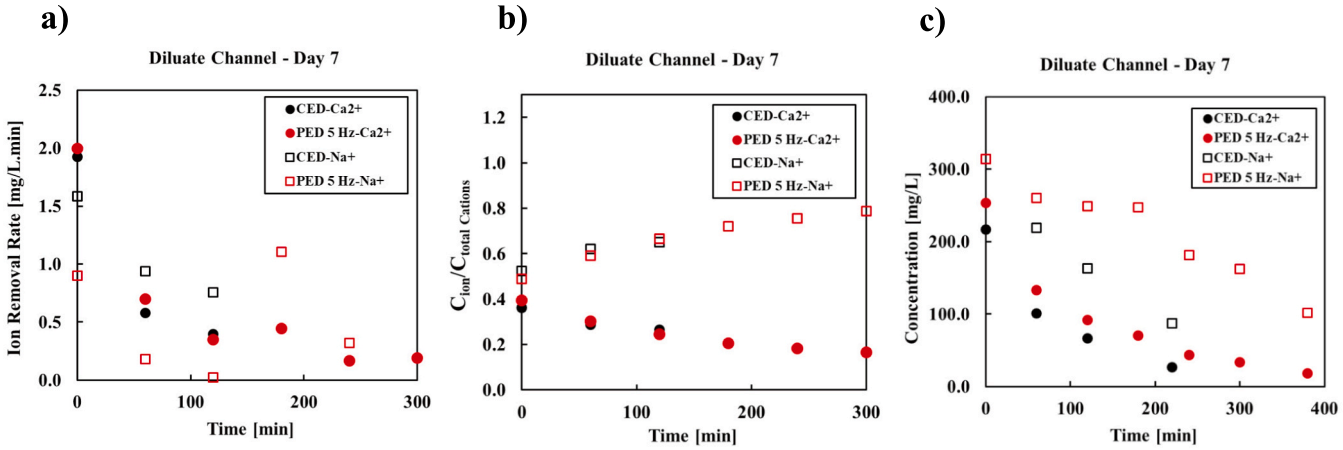

Fig. 14. Evaluation of the effects of 5 Hz pulsing on the evolution of solution composition during day seven of the nine-day desalination batch experiments. Comparison of (**a**) Ca^{2+} and Na^+ removal rates, (**b**) Ca^{2+} and Na^+ concentration ratio over existing cations, (**c**) Ca^{2+} and Na^+ diluate bulk concentrations in PED and CED.

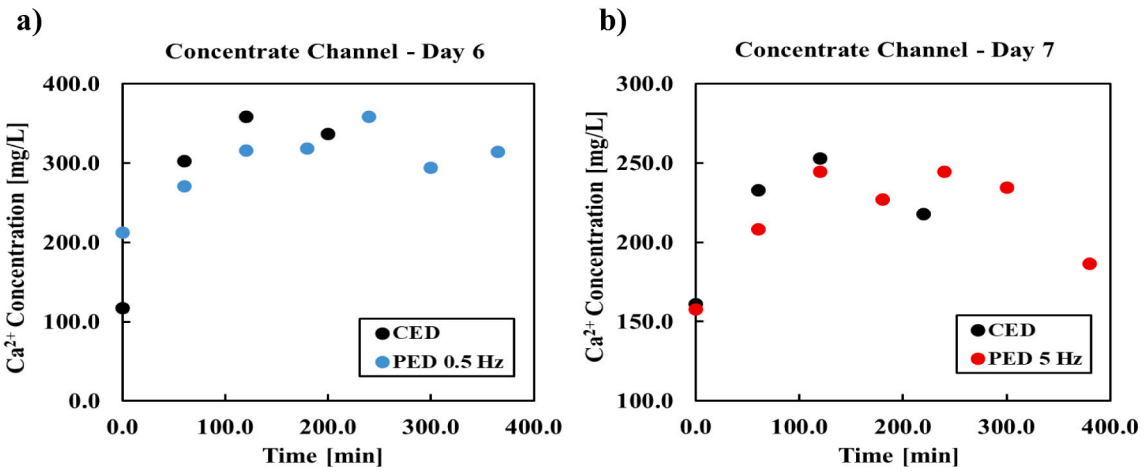

Fig. 15. Comparison of Ca^{2+} concentrate bulk concentrations in CED and PED with the frequency of 0.5 Hz during day six of nine-day batch experiments **(a)** and in CED and PED with the frequency of 5 Hz during day seven of nine-day batch experiments **(b)**.

compartments can affect the morphology of the formed crystals in addition to changing the crystal nucleation and growth rates. As indicated in the SEM images (Figs. 8 and 10) and EDX analyses (Figs. 9 and 11), aragonite formation was more dominant in CED and PED with the frequency of 5 Hz. Prior studies [49,50] indicated that the extent of aragonite formation in the system depended on a number of parameters including the supersaturation degree of the concentrate solution as well as the Mg^{2+} to Ca^{2+} concentration ratio. It was elucidated that a greater supersaturation and higher concentrations of Mg^{2+} ions in the solution favored the formation of aragonite over calcite. As demonstrated in Fig. 16, the Mg^{2+} to Ca^{2+} concentration ratio (calculated based on ICP-OES data) was greater in the concentrate channels of CED and PED with the frequency of 5 Hz, resulting in the dominance of metastable aragonite polymorph under these operational conditions. As discussed earlier, the higher transport rates of Ca^{2+} in CED and PED with the frequency of 5 Hz compared to that of PED with the frequency of 0.5 Hz led to potentially greater supersaturation, further promoting aragonite formation under the higher frequency operational condition.

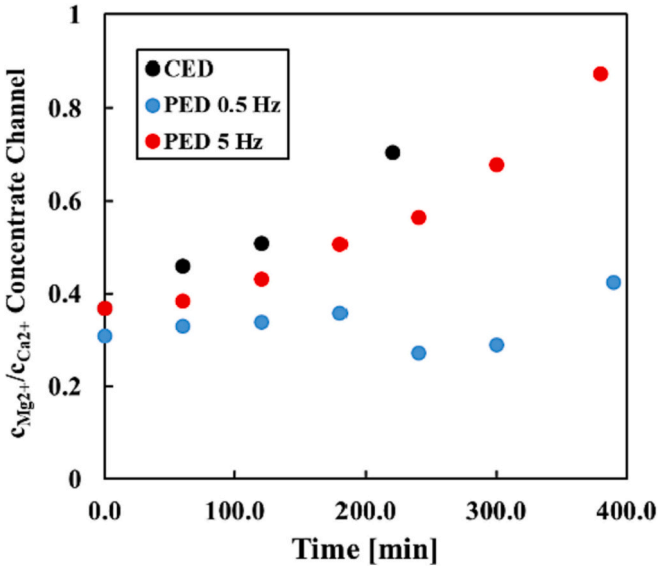

Fig. 16. Mg^{2+} to Ca^{2+} concentration ratio in the concentrate channel during day seven of the nine-day desalination batch experiments in CED and PED with the duty cycle of 50 %, calculated using ICP-OES measurements. The imposed voltage under all operational conditions was 4.5 V.

5. Pulsed operation as a chemical-free scale mitigation strategy

Our analyses elucidated the effects of pulsing parameters on the evolution of concentration distributions of scaling and non-scaling ions in the ED stack and their potential effects on salt formation kinetics. Depending on the on and off durations, pulsing can mitigate scale formation by decreasing the transport rate of scale-forming ions to the concentrate compartment, reducing the concentration build-up in CBL, and eliminating the emerged nuclei with the longitudinal flow. In the system studied here, pulsing with the frequency of 0.5 Hz reduced membrane scaling and indicated potential usability as a chemical-free scale mitigation strategy especially once combined with finer pre-filtration units to avoid bulk crystallization. According to the insight gained here, three main factors should be considered in selecting pulsing parameters including feedwater composition (the divalent to monovalent ions concentration ratio), the channel velocity, and the residence time of the solution inside the ED stack. While feedwater composition determines the selective transport of scale-forming ions over monovalent ions, the cell hydrodynamics (channel velocity and associated BL thickness) informs the time required for retrieving the concentration profiles in the boundaries. To be truly useful, pulsing parameters should be adjusted with respect to the residence time of the solution inside the stack to ensure at least one full cycle of pulsing occurs within a single pass of water through the unit.

The developed simplified ion transport model is a useful tool to determine the pulsing duration by calculating the divalent and monovalent ions fluxes at different time steps for various feedwater chemistries. The effects of channel velocity can be implemented in the model by tuning the thickness of boundary layers. Even though various divalent ions may impose separate scaling issues, lumping solution chemistry into divalent and monovalent ion groups provides a computationally simple yet effective estimation of the concentration distribution of scale-forming ions in the concentrate channel. Using the developed model for the selection of pulsing parameters eliminates the need for trial-and-error approaches, improving the viability and generalizability of the pulsed operation for scale mitigation. According to the results of this study, low-frequency pulsing is more effective in reducing the transport rate of scale-forming components from the diluate channel and controlling the super-saturation of the concentrate compartment. However, at the duty cycle of 50 %, care must be taken when using an extremely small frequency to avoid full polarization of scale-forming components in the boundaries during long on-times.

One of the limitations of applying pulsed operation is the increase in desalination time which adversely affects the energy efficiency of the system (higher pumping energy) and results in a longer available period

for salt to precipitate out of the metastable supersaturated solution in the concentrate channel. For the synthesized brackish water in this study, due to the higher selectivity of ED toward the transport of multivalent ions, the majority of the Ca^{2+} ions were removed from the diluate channel within approximately the first 50 % of the batch duration, as indicated in Figs. 13 and 14. Therefore, continuing with pulsed operation within the second half of the batch is expected to have minimal effects on controlling the concentration build-up of the scale-forming ions in the concentrate channel while increasing the desalination time and energy. As indicated in Fig. 15, the decrease in Ca^{2+} concentration took place approximately in the second half of the batch in the concentrate channel of PED, indicating that salt formation was taking place. Hence, modification of pulsed operation to reduce the time of the batch can both improve the energy efficiency and scaling mitigation in the system, further enhancing the viability of the approach.

5.1. *Hybrid pulsed-conventional operation with improved performance*

To improve the desalination rate of PED while preserving its scale mitigation properties, we propose a novel hybrid pulsed-conventional operation (PED-CED) in which the electric field is only pulsed for a predetermined percentage of a batch before transitioning to conventional operation. A PED-CED system provides the opportunity to leverage the advantages of pulsing in moderating divalent ion transport from diluate to concentrate channels, which is higher earlier in the batch while reducing the overall time of desalination compared to a pure PED system by switching to CED later in the process. The shorter time of a PED-CED batch compared to a pure PED also decreases the recirculation period of the saturated concentrate streams through the stack, potentially decreasing crystal growth and deposition.

For a PED-CED system, the selection of the optimum percentage for the transition from pulsed to conventional operation depends on the salinity and composition of the solution as well as the batch time and energy consumption of PED relative to CED. To conduct a preliminary evaluation, the batch time and SEC of PED-CED at different transition percentages (Fig. 17a and b) were estimated by using the data for the PED (f = 0.5 Hz) and CED batches presented in Fig. 6a and b. The percentage of the batch spent pulsing is calculated as $\frac{c^t - c^F}{c^i - c^F}$, where c^t is the salinity at time t, c^F is the final salinity, and c^i is the initial salinity. With this methodology, the performance of PED-CED at a batch transition percentage of 25 % is estimated by adding the batch time and SEC of the first 25 % of a PED batch and the last 75 % of a CED batch. Our estimation indicates that the PED-CED with a transition percentage of 50 % only increases the batch time by ~25 % relative to pure CED, much lower than the 75 % batch time increase observed for pure PED (Fig. 17a). As indicated from ICP-OES data (Fig. 13c), the majority of Ca^{2+} was transported to the concentrate channel within the first 50 % of the PED batch. Thus, transitioning to conventional operation after 50 % spent pulsing has no effect on modulating the transport rate of scale-forming ions to the concentrate channel while significantly decreasing the batch time relative to the pure PED. The SEC of the hybrid system is slightly lower than both conventional or pulsed processes (Fig. 17b).

PED-CED operation can potentially decrease surface and bulk crystallization compared to the pure PED system due to the relative reduction in batch time and shortening of the period during which the highly concentrated brine solution is recirculated through the stack. Hence, it is expected that direct implementation of the PED-CED operation achieves even lower energy consumption compared to calculated values using the pure CED and PED data (Fig. 17b). Furthermore, decreasing the batch time through PED-CED reduces the required pumping energy relative to pure PED operation, enhancing the viability of pulsing as a scale-mitigation approach. Investigating the performance of the PED-CED system and the dependence of the transition percentage on the solution composition are the subjects of future studies.

6. Conclusions

In this study, we investigated the effects of the pulsed operation of electrodialysis on mitigating concentration polarization and reducing membrane scaling in the desalination of synthesized brackish water with a high scaling propensity. We used our theoretical model to estimate the effective pulsing frequencies (0.5 and 5 Hz), taking into account their impacts on the fluxes of scale-forming ions. The duty cycle of pulsing was set to 50 % and the imposed voltage of PED was the same as that of CED to keep the desalination time and energy consumption low. A single desalination experiment was conducted daily at an 80 % recovery ratio for nine consecutive days to investigate the effects of long-term, intermittent batch operation on scale formation. The extent of salt formation was quantified by measuring SEC and pressure drops for each batch followed by performing spectroscopy and microscopic analyses of the membranes removed from the stack at the end of the nine-day desalination period.

Our results demonstrated that the choice of pulsing parameters

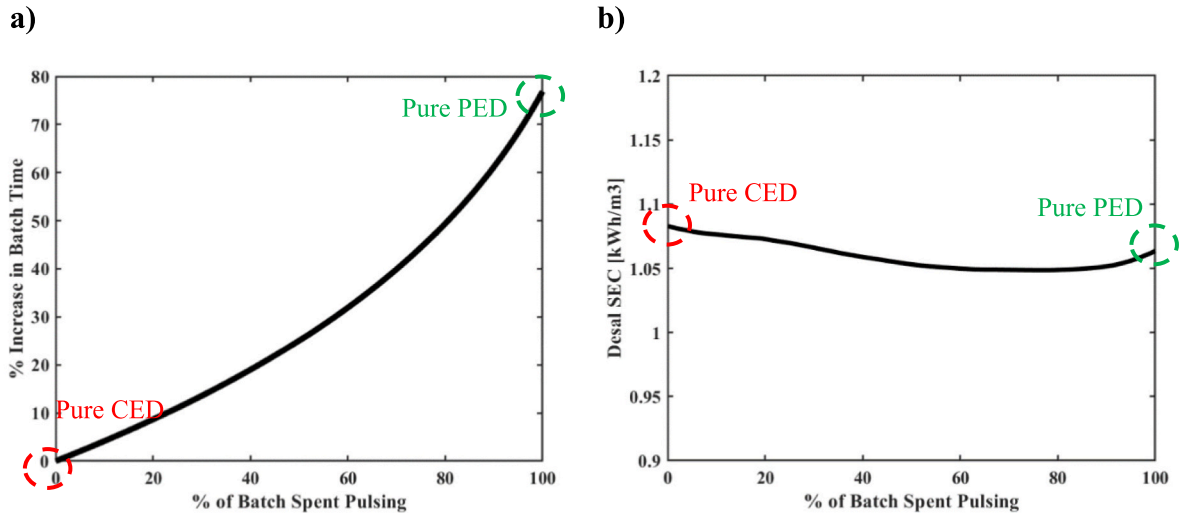

Fig. 17. Evaluation of batch time and specific energy consumption of a hybrid PED-CED system. **a)** Calculated increases in batch time. **b)** The specific energy consumption (SEC) of the PED-CED system versus the percentage of the batch spent pulsing. The values presented in the figures are calculated using the experimentally measured batch time and SEC of pure CED and pure PED (0.5 Hz and 50 % duty cycle) for desalination of synthesized brackish water from 2000 to 250 mg/L at 4.5 V.

affected the rate of crystal formation and growth, resulting in various quantities of surface and bulk crystallization of $CaCO_3$. Under all pulsing conditions, less salt formation was observed on the surface of the membranes in PED compared to those in CED. High-frequency pulsing (5 Hz) increased the rate of divalent ion transport across the membranes. Hence, the higher supersaturation degree of the solution combined with shorter concentration recovery periods decreased the effectiveness of pulsing in eliminating surface crystallization. Pulsing with a low frequency (0.5 Hz) was more successful in reducing membrane clogging by decreasing the transport rate of scale-forming ions to the concentrate channel, reducing the supersaturation and potentially the crystal nucleation rates in the boundary layers. However, bulk crystallization and colloidal fouling increased at the frequency of 0.5 Hz, necessitating the use of finer pre-filtration units to remove the suspended crystal from the solution before recirculation. Under all operational conditions, the transport of scale-forming Ca^{2+} ions occurred within the first ~50 % of the batch time, indicating the selectivity of ED toward the transport of divalent ions earlier in the desalination process.

To improve the feasibility of the pulsed operation as a scale mitigation strategy, we proposed a hybrid PED-CED system that leveraged the benefits of pulsing for controlling the transport rates of scale-forming ions earlier in the batch and improved the DR by switching to the conventional operation later in the process. Our preliminary analyses of the hybrid pulsed-conventional ED system, performed using the collected data for the pure CED and PED systems, indicated a significant reduction in desalination time compared to the pure PED. The use of the hybrid pulsed-conventional operation for the desalination of brackish water could decrease bulk and surface crystallization.

Even though the range of pulsing parameters studied here can potentially be appropriate for any brackish water with a similar salinity range, further analyses need to be conducted to verify the effectiveness of the selected pulsing parameters. The compositional dependence needs to be examined using different water chemistries with varying supersaturation degrees and precipitating salts. The parametric understanding gained through this study shed light on the existing knowledge gap on the performance of PED and provides further avenues for improvement that can potentially enhance the viability of the approach as a scale mitigation strategy in desalination of brackish water at high recoveries.

CRediT authorship contribution statement

S. Honarparvar: Investigation, design of experiment, the conduct of experiments & data acquisition, data analysis & interpretation, development of the modeling framework, writing- the original draft, writing-review & editing.

R. Al-Rashed: Investigation, design of experiment, the conduct of experiments & data acquisition, data analysis & interpretation, writing-the original draft, writing- review & editing.

A. G. Winter: Conceptualization and design of the study, funding acquisition, project administration, resources, supervision, review of the collected data and the modeling results, review & revision of the manuscript.

Declaration of competing interest

The authors declare that they have no known competing financial interests or personal relationships that could have appeared to influence the work reported in this paper.

Data availability

The modeling results and experimental data are provided in the manuscript.

Acknowledgment

This work was sponsored by the United States Bureau of Reclamation Desalination and Water Purification Research and Development Program grant R19AC00104, and Kuwait University.

Appendix A

Table A1
A summary of solution compositions and pulsing conditions used in scaling/fouling mitigation studies with PED.

Authors	System under study	Voltage/current	Frequency (Hz)	Duty cycle, %
Lee et al. [33]	DC: 0.05 mol/L of NaCl solution with 0.01 wt% sodium humate CC: 0.05 mol/L NaCl solution	6 mA/cm^2	60, 100, 200	50
Lee et al. [34]	DC: 80 g/L of sodium lactate with 1 wt% bovine serum albumin (BSA) CC: 30 g/L of sodium lactate	6 mA/cm^2	10, 25, 50, 100, 200	50
Lee et al. [32]	DC: fermentation waste containing Cl^-, SO_4^{2-}, NH_4^+, K^+, Mg^{2+}, Ca^{2+} CC: solution containing 6.9 g/L $(NH_4^+)_2SO_4$ and 1.9 g/L $(K)_2SO_4$	25 mA/cm^2 (~0.3 i_{lim})	The half-wave power generated from AC	50
Lee and Moon, [31]	DC: 0.1 mol/L of NaCl solution containing 0.1 g/L sodium humate CC: 0.05 mol/L NaCl solution	6 mA/cm^2	10, 25, 50, 100, 200	50
Ruiz et al. [29]	DC: 1 g/L of Na_2CO_3, 0.8 g/L of KCl, 0.8 g/L of $CaCl_2$, 32 g/L of protein CC: 2 g/L KCl solution with basic pH	10, 20, and 30 mA/cm^2 ($\sim 0.6i_{lim} < i < \sim 2i_{lim}$)	0.02, 0.05	20, 50
Casademont et al. [21]	DC: 1 g/L of Na_2CO_3, 0.8 g/L of KCl, 0.8 g/L of $CaCl_2$, 0.113 g/L of $MgCl_2$, 32.6 g/L of whey protein isolates CC: pH controlled 20 g/L NaCl solution	15 mA/cm^2 ($0.75i_{lim}$)	0.02	20
Cifuentes-Araya et al. [22–25]	DC: 1 g/L of Na_2CO_3, 0.8 g/L of KCl, 0.8 g/L of $CaCl_2$, 0.452 g/L of $MgCl_2$ CC: pH controlled 2 g/L of KCl solution	40 mA/cm^2	0.023, 0.033, 0.05, 0.067, 0.1	23, 23.1, 33.3, 50, 66.7
Mikhaylin et al. [28]	DC: 1 g/L of Na_2CO_3, 0.8 g/L of KCl, 0.8 g/L of $CaCl_2$, 0.452 g/L of $MgCl_2$ CC: pH controlled 2 g/L KCl solution	40 mA/cm^2	0.75, 0.5, 0.4, 0.37, 0.3, 0.25	75.2, 50, 0.8, 0.75, 0.9, 0.75
Andreeva et al. [35]	DC: 1 g/L of Na_2CO_3, 0.8 g/L of KCl, 4.116 g/L of $CaCl_2{\cdot}2H_2O$, 2.440 g/L of $MgCl_2.6H_2O$ CC: pH controlled 0.04 mol/L NaCl solution	$i_{lim}^{exp} < i < 2i_{lim}^{exp}$	0.00056, 0.00074, 0.0017, 0.0083	50, 66.7
Lemay et al. [36]	DC: sweet whey solution CC: pH controlled 2 g/L KCl solution	8 mA/cm^2 ($0.6i_{lim}$)	5, 0.91, 0.5, 0.1, 0.09, 0.05, 0.01	50, 91, 99
Merkel and Ashrafi, [27]	DC: whey solution CC: tap water	50 V during pulse & −50 V during reverse	0.0055, 0.029	98.4, 85.7
Dufton et al. [26]	DC: acid whey solution containing Na^+, K^+, Mg^{2+}, Ca^{2+}, P^{3-} CC: 5.5 g/L NaCl solution	100 mA/cm^2 ($0.8i_{lim}$)	0.017, 0.02	50, 83.3

(*continued on next page*)

Table A1 (*continued*)

Authors	System under study	Voltage/current	Frequency (Hz)	Duty cycle, %
Lemay et al. [37]	DC: sweet whey solution CC: pH controlled 2 g/L KCl solution	8 mA/cm^2 ($0.6i_{lim}$)	0.5, 5	50
Gao et al. [38]	DC: sodium gluconate mother liquid CC: deionized water	9 V	0.2	80
Sosa-Fernandez et al. [39]	Synthesized brackish water (53.3 mmol/L of NaCl, 15.53 mmol/L of $NaHCO_3$, 0.72 mmol/L of KCl, 2.51 mmol/L of Na_2SO_4, 0.65 mmol/L of $CaCl_2{\cdot}2H_2O$, 0.46 mmol/L of $MgCl_2{\cdot}6H_2O$) + 250 mg/L of hydrolyzed polyacrylamide (HPAM) + 2 mg/L of crude oil	i = 32 A/cm^2 ($0.55i_{lim}$)	0.0025, 0.005, 0.025, 0.05, 0.25, 0.5, 5 & back pulse: t_{back} = 0.1 s, t_{off} = 49.9 s	50, 25, 75

DC: diluate channel, CC: concentrate channel.

References

[1] J.S. Stanton, et al., Brackish groundwater in the United States, in: US Geological Survey, 2017, pp. 2330–7102.
[2] M. Myint, A. Ghassem, N. Nirmalakhandan, Low energy/cost desalination: low dose and low mean ion resident time in concentrate stream of electro-dialysis reversal, Water Sci. Technol. 63 (9) (2011) 1855–1863.
[3] J. Li, M. Tang, Z. Ye, L. Chen, Y. Zhou, Scale formation and control in oil and gas fields: a review, J. Dispers. Sci. Technol. 38 (5) (2017) 661–670.
[4] S. Najibi, H. Müller-Steinhagen, M. Jamialahmadi, Calcium sulphate scale formation during subcooled flow boiling, Chem. Eng. Sci. 52 (8) (1997) 1265–1284.
[5] S. Honarparvar, X. Zhang, T. Chen, A. Alborzi, K. Afroz, D. Reible, Frontiers of membrane desalination processes for brackish water treatment: a review, Membranes 11 (4) (2021) 246.
[6] E. Jones, M. Qadir, M.T. van Vliet, V. Smakhtin, S.-M. Kang, The state of desalination and brine production: a global outlook, Sci. Total Environ. 657 (2019) 1343–1356.
[7] Y.D. Ahdab, G.P. Thiel, J.K. Böhlke, J. Stanton, J.H. Lienhard, Minimum energy requirements for desalination of brackish groundwater in the United States with comparison to international datasets, Water Res. 141 (2018) 387–404.
[8] S.K. Patel, P.M. Biesheuvel, M. Elimelech, Energy consumption of brackish water desalination: identifying the sweet spots for electrodialysis and reverse osmosis, ACS ES&T Engineering 1 (2021) 851–864.
[9] W.E. Katz, The electrodialysis reversal (EDR) process, Desalination 28 (1) (1979) 31–40.
[10] M.Y. Ashfaq, M.A. Al-Ghouti, D.A. Da'na, H. Qiblawey, N. Zouari, Effect of concentration of calcium and sulfate ions on gypsum scaling of reverse osmosis membrane, mechanistic study, J. Mater. Res. Technol. 9 (6) (2020) 13459–13473.
[11] M. Çelikbilek, A.E. Ersundu, S. Aydın, Crystallization kinetics of amorphous materials, Adv. Crystall. Processes 35347 (2012).
[12] M. Hansima, et al., Fouling of ion exchange membranes used in the electrodialysis reversal advanced water treatment: a review, Chemosphere 263 (2021), 127951.
[13] M. Vaselbehagh, H. Karkhanechi, R. Takagi, H. Matsuyama, Effect of polydopamine coating and direct electric current application on anti-biofouling properties of anion exchange membranes in electrodialysis, J. Membr. Sci. 515 (2016) 98–108.
[14] A.T. Tran, N. Jullok, B. Meesschaert, L. Pinoy, B. Van der Bruggen, Pellet reactor pretreatment: a feasible method to reduce scaling in bipolar membrane electrodialysis, J. Colloid Interface Sci. 401 (2013) 107–115.
[15] V. Hábová, K. Melzoch, M. Rychtera, B. Sekavová, Electrodialysis as a useful technique for lactic acid separation from a model solution and a fermentation broth, Desalination 162 (2004) 361–372.
[16] D.Y. Butylskii, V. Troitskiy, M. Sharafan, N. Pismenskaya, V. Nikonenko, Scaling-resistant anion-exchange membrane prepared by in situ modification with a bifunctional polymer containing quaternary amino groups, Desalination 537 (2022), 115821.
[17] Y. Zhao, et al., Composite anti-scaling membrane made of interpenetrating networks of nanofibers for selective separation of lithium, J. Membr. Sci. 618 (2021), 118668.
[18] J. Zhao, Q. Chen, L. Ren, J. Wang, Fabrication of hydrophilic cation exchange membrane with improved stability for electrodialysis: an excellent anti-scaling performance, J. Membr. Sci. 617 (2021), 118618.
[19] W. Garcia-Vasquez, R. Ghalloussi, L. Dammak, C. Larchet, V. Nikonenko, D. Grande, Structure and properties of heterogeneous and homogeneous ion-exchange membranes subjected to ageing in sodium hypochlorite, J. Membr. Sci. 452 (2014) 104–116.
[20] W. Garcia-Vasquez, L. Dammak, C. Larchet, V. Nikonenko, D. Grande, Effects of acid–base cleaning procedure on structure and properties of anion-exchange membranes used in electrodialysis, J. Membr. Sci. 507 (2016) 12–23.
[21] C. Casademont, P. Sistat, B. Ruiz, G. Pourcelly, L. Bazinet, Electrodialysis of model salt solution containing whey proteins: enhancement by pulsed electric field and modified cell configuration, J. Membr. Sci. 328 (1–2) (2009) 238–245.
[22] N. Cifuentes-Araya, G. Pourcelly, L. Bazinet, Impact of pulsed electric field on electrodialysis process performance and membrane fouling during consecutive demineralization of a model salt solution containing a high magnesium/calcium ratio, J. Colloid Interface Sci. 361 (1) (2011) 79–89.
[23] N. Cifuentes-Araya, G. Pourcelly, L. Bazinet, Water splitting proton-barriers for mineral membrane fouling control and their optimization by accurate pulsed modes of electrodialysis, J. Membr. Sci. 447 (2013) 433–441.
[24] N. Cifuentes-Araya, G. Pourcelly, L. Bazinet, How pulse modes affect proton-barriers and anion-exchange membrane mineral fouling during consecutive electrodialysis treatments, J. Colloid Interface Sci. 392 (2013) 396–406.
[25] N. Cifuentes-Araya, G. Pourcelly, L. Bazinet, Multistep mineral fouling growth on a cation-exchange membrane ruled by gradual sieving effects of magnesium and carbonate ions and its delay by pulsed modes of electrodialysis, J. Colloid Interface Sci. 372 (1) (2012) 217–230.
[26] G. Dufton, S. Mikhaylin, S. Gaaloul, L. Bazinet, Positive impact of pulsed electric field on lactic acid removal, demineralization and membrane scaling during acid whey electrodialysis, Int. J. Mol. Sci. 20 (4) (2019) 797.
[27] A. Merkel, A.M. Ashrafi, An investigation on the application of pulsed electrodialysis reversal in whey desalination, Int. J. Mol. Sci. 20 (8) (2019) 1918.
[28] S. Mikhaylin, V. Nikonenko, G. Pourcelly, L. Bazinet, Intensification of demineralization process and decrease in scaling by application of pulsed electric field with short pulse/pause conditions, J. Membr. Sci. 468 (2014) 389–399.
[29] B. Ruiz, P. Sistat, P. Huguet, G. Pourcelly, M. Araya-Farias, L. Bazinet, Application of relaxation periods during electrodialysis of a casein solution: impact on anion-exchange membrane fouling, J. Membr. Sci. 287 (1) (2007) 41–50.
[30] S. Suwal, J. Amiot, L. Beaulieu, L. Bazinet, Effect of pulsed electric field and polarity reversal on peptide/amino acid migration, selectivity and fouling mitigation, J. Membr. Sci. 510 (2016) 405–416.
[31] H.-J. Lee, S.-H. Moon, Enhancement of electrodialysis performances using pulsing electric fields during extended period operation, J. Colloid Interface Sci. 287 (2) (2005) 597–603.
[32] H.-J. Lee, S.-J. Oh, S.-H. Moon, Recovery of ammonium sulfate from fermentation waste by electrodialysis, Water Res. 37 (5) (2003) 1091–1099.
[33] H.-J. Lee, S.-H. Moon, S.-P. Tsai, Effects of pulsed electric fields on membrane fouling in electrodialysis of NaCl solution containing humate, Sep. Purif. Technol. 27 (2) (2002) 89–95.
[34] H.-J. Lee, J.-S. Park, S.-H. Moon, A study on fouling mitigation using pulsing electric fields in electrodialysis of lactate containing BSA, Korean J. Chem. Eng. 19 (5) (2002) 880–887.
[35] M. Andreeva, et al., Mitigation of membrane scaling in electrodialysis by electroconvection enhancement, pH adjustment and pulsed electric field application, J. Membr. Sci. 549 (2018) 129–140.
[36] N. Lemay, S. Mikhaylin, L. Bazinet, Voltage spike and electroconvective vortices generation during electrodialysis under pulsed electric field: impact on demineralization process efficiency and energy consumption, Innovative Food Sci. Emerg. Technol. 52 (2019) 221–231.
[37] N. Lemay, S. Mikhaylin, S. Mareev, N. Pismenskaya, V. Nikonenko, L. Bazinet, How demineralization duration by electrodialysis under high frequency pulsed electric field can be the same as in continuous current condition and that for better performances? J. Membr. Sci. 603 (2020) 1–12, 117878.
[38] Q. Gao, et al., Application of pulsed electric field in antifouling treatment of sodium gluconate mother liquor by electrodialysis, Materials 13 (11) (2020) 2501.
[39] P. Sosa-Fernandez, J. Post, M. Ramdlan, F. Leermakers, H. Bruning, H. Rijnaarts, Improving the performance of polymer-flooding produced water electrodialysis through the application of pulsed electric field, Desalination 484 (2020), 114424.
[40] S. Honarparvar, R. Al-Rashed, A.G. Winter, A comprehensive investigation of performance of pulsed electrodialysis for desalination of brackish water, Desalination 547 (2023), 116240.
[41] S. Mikhaylin, L. Bazinet, Fouling on ion-exchange membranes: classification, characterization and strategies of prevention and control, Adv. Colloid Interf. Sci. 229 (2016) 34–56.
[42] J. Mackie, P. Meares, The diffusion of electrolytes in a cation-exchange resin membrane I. Theoretical, Proc. R. Soc. Lond. A Math. Phys. Sci. 232 (1191) (1955) 498–509.
[43] M.A.-K. Urtenov, E.V. Kirillova, N.M. Seidova, V.V. Nikonenko, Decoupling of the Nernst– planck and poisson equations. Application to a membrane system at overlimiting currents, J. Phys. Chem. B 111 (51) (2007) 14208–14222.
[44] S.-X. Bao, Y.-M. Zhang, T. Liu, J. Huang, T.-J. Chen, Evolution and morphometric characterization of fouling on membranes during the desalination of high CaSO4 supersaturated water by electrodialysis, Desalination 256 (1–3) (2010) 94–100.

[45] A. Antony, J.H. Low, S. Gray, A.E. Childress, P. Le-Clech, G. Leslie, Scale formation and control in high pressure membrane water treatment systems: a review, J. Membr. Sci. 383 (1–2) (2011) 1–16.
[46] A. Neira, M.S. Fernández, J. Retuert, J.L. Arias, Effect of the crystallization chamber design on the polymorphs of calcium carbonate using the sitting-drop method, in: Materials Research Society: Warrendale, PA, 2004.
[47] A.W. Ritchie, et al., Reversed crystal growth of rhombohedral calcite in the presence of chitosan and gum arabic, CrystEngComm 15 (47) (2013) 10266–10271.
[48] P. Moulin, H. Roques, Zeta potential measurement of calcium carbonate, J. Colloid Interface Sci. 261 (1) (2003) 115–126.
[49] R.L. Curl, The Aragonite-Calcite Problem, 1962.
[50] M. Boon, W.D. Rickard, A.L. Rohl, F. Jones, Stabilization of aragonite: role of Mg2 + and other impurity ions, Cryst. Growth Des. 20 (8) (2020) 5006–5017.